JOURNAL OF GEOPHYSICAL RESEARCH, VOL. 112, C04022, doi:10.1029/2006JC003493, 2007

Summer landfast sea ice desalination at Point Barrow, Alaska: Modeling and observations

Martin Vancoppenolle,[1] Cecilia M. Bitz,[2] and Thierry Fichefet[1]

Received 17 January 2006; revised 28 September 2006; accepted 19 October 2006; published 28 April 2007.

[1] Landfast sea ice cores from two sites in Point Barrow, Alaska, extracted between 1999 and 2001, show a progressive desalination and a corresponding shape transition in the salinity profile starting at snowmelt onset, around 1 June. The vertical percolation of fresh surface meltwater through the permeable ice matrix (flushing) has long been supposed to control this transition. A parameterization of flushing in bare ice is formulated. It is incorporated into the semiempirical winter sea ice desalination model of Cox and Weeks (1988), coupled to the one-dimensional thermodynamic sea ice model of Bitz and Lipscomb (1999) and forced under Point Barrow conditions. Adjustment to the original Cox and Weeks parameterization of gravity drainage was necessary to give reasonable agreement with observations in winter. With this change the model has the potential to simulate the full seasonal cycle of the Arctic salinity and mass balance of typical Arctic ice. In summer, the model salinity profile closely follows the observations. The model upper ice temperatures are slightly too cold. At the thin snow (Chukchi Sea) site, the model simulates the observed snow depth and ice thickness well. At the thick snow (Elson Lagoon) site, the snow disappears 7 days earlier than observed, which results in underestimating ice thickness. Sensitivity experiments suggest that a more realistic representation of snow and meltwater physics would significantly improve the simulation. Because of the effects of brine drainage on the sea ice mass balance and oceanic circulation, including the time dependence of the ice salinity profile would significantly improve the next generation of sea ice models.

Citation: Vancoppenolle, M., C. M. Bitz, and T. Fichefet (2007), Summer landfast sea ice desalination at Point Barrow, Alaska: Modeling and observations, *J. Geophys. Res.*, *112*, C04022, doi:10.1029/2006JC003493.

1. Introduction

1.1. Importance of Sea Ice and Its Salinity

[2] Sea ice acts as a damping membrane between atmosphere and ocean, modulating exchanges between them in polar regions. Transfer of radiation (through high albedo), momentum, heat (through low thermal conductivity) and mass (through freshwater and tracers) exchanges are affected.

[3] Sea ice is a saline medium. A fraction of oceanic salt is trapped in the ice during formation, while the remainder is rejected into the ocean. The salt in sea ice is not locked within the ice crystalline lattice, but dissolved within liquid inclusions of brine. As this brine is progressively drained, the ice desalinates [*Cox and Weeks*, 1974; *Weeks and Ackley*, 1986].

[4] The ice salinity affects sea ice thermodynamic properties. First, each part per thousand (‰) of sea ice salinity lowers the seawater freezing point by 0.054°C [*Assur*, 1958]. Second, the phase composition of sea ice depends on salinity and temperature. The saltier and warmer the ice, the larger the relative brine volume [*Frankenstein and Garner*, 1967]. Thus the sea ice thermal properties depend on salinity and temperature [*Malmgren*, 1927; *Untersteiner*, 1964; *Ono*, 1967]. The thermal properties regulate growth and melt rates at the ice interfaces, as well as the vertical temperature profile in the ice. In particular, in the Arctic, the sea ice salinity close to the surface seems to be a key factor, since it influences the summer melt rate and equilibrium multiyear ice (MY) thickness through a prominent control of heat transfer and storage in the ice [*Vancoppenolle et al.*, 2005]. Ice with lower near surface salinity has reduced heat conduction, less internal brine pocket melting and more surface ablation.

[5] The scope of the role of sea ice salinity actually goes beyond its influence on sea ice thermodynamics, as it is now largely accepted that the brine volume connectivity influences the nutrient supply for the microorganisms and algae living in sea ice [*Ackley and Sullivan*, 1994]. In addition, the size and shape distribution of brine inclusions affect shortwave radiation scattering [*Perovich*, 1998; *Light et al.*, 2003] and strength and mechanical behavior [*Timco and Frederking*, 1990; *Kovacs*, 1997] in the ice. Sea ice salinity indirectly controls growth/melt rates and thus freshwater and brine exchanges between ice and ocean [*Vancoppenolle et al.*, 2005]. The salt/freshwater fluxes associated with ice

---

[1] Institut d'Astronomie et de Géophysique G. Lemaître, Université Catholique de Louvain, Louvain-la-Neuve, Belgium.

[2] Department of Atmospheric Sciences, University of Washington, Seattle, Washington, USA.

0148-0227/07/2006JC003493$09.00

growth/melt have a strong impact on the oceanic salinity stratification, critical to the circulation of the high-latitude ocean and the World Ocean thermohaline circulation [*Aagaard and Carmack*, 1989]. In summer, the meltwater pathways and storage at the ice surface, driven by the ice salinity-dependent permeability structure, regulate the size of melt ponds, and, in turn, surface albedo [*Eicken et al.*, 2002, 2004]. Finally, the sea ice salinity affects the carbon cycle in polar regions. *Semiletov et al.* [2004] reported that open brine channels form an important spring/summer CO_2 pathway to the Arctic Ocean. This is corroborated by recent observations in the ice pack off the Adélie-Wilkes Coast (spring) and in the Weddell Sea (summer), which show significant carbon fluxes between atmosphere and ocean through the sea ice, primarily modulated by a very dynamic biogeochemistry. The latter appears to be extremely sensitive to the brine network connectivity, which shows drastic changes around the 5% brine volume threshold (J. L. Tison and B. Delille, personal communication, 2006).

1.2. Observations of Ice Salinity

[6] The sea ice salinity profile evolves in space and time [*Malmgren*, 1927; *Eicken*, 1998]. The bulk salinity decreases with time as the ice thickens, as indicated by the significant salinity versus thickness relationships [*Cox and Weeks*, 1974; *Kovacs*, 1996].

[7] In the Arctic, first-year (FY) ice has a C-shaped salinity profile [see, e.g., *Nakawo and Sinha*, 1981]. A first, rapid desalination stage is observed to occur in the first two weeks of ice formation, bringing the ice salinity from around 20‰ to roughly 10‰, by the time the ice is around 30 cm thick. Then, a second, slower, desalination stage, occurs during the remainder of winter, bringing the ice salinity to around 5–6‰, by the beginning of its first melt season [*Kovacs*, 1996].

[8] MY ice, which has experienced summer melt at least once, has a different salinity profile. The upper 50 cm of the ice are almost fresh. Below the fresh layer, the salinity increases quickly with depth and reaches a maximum typically of 4‰. Very similar MY ice salinity profiles have been found at different locations [e.g., *Schwarzacher*, 1959; *Tucker et al.*, 1987; *Eicken et al.*, 1995]. Therefore the MY ice salinity profile has been hypothesized to be very stable in time and often has been referred to as the MY equilibrium salinity profile [*Schwarzacher*, 1959; *Untersteiner*, 1968]. Although the distinction between FY and MY salinity profiles is well documented, the desalination mechanism that causes the transition has received little attention, as outlined by *Weeks* [1998]. Only a few Arctic early summer salinity profiles are documented in the literature. On the basis of 51 FY ice cores taken from the Fram Strait region, *Tucker et al.* [1987] show a gradual and intense desalination takes place from June to July.

[9] In the Southern Ocean, the situation is quite different. Overall, Antarctic sea ice is slightly more saline (between 0.5 and 1.0‰) than its Arctic counterpart, as observed in the Weddell Sea [*Gow et al.*, 1982; *Gow et al.*, 1987]. In addition, salinity profiles around Antarctica have more variable shape [*Eicken*, 1992], probably due to intense rafting, surface flooding and snow ice formation [*Maksym and Jeffries*, 2000]. Furthermore, very little difference between FY and MY salinity profile shapes have been seen, as indicated by a study of 89 sample cores extracted from winter Weddell Sea ice by *Eicken* [1998]. The lack of surface melt in summer [*Andreas and Ackley*, 1981] alone might keep the surface layer in Antarctic relatively saline compared to Arctic MY ice surface layer in Antarctic MY ice. However, *Haas et al.* [2001] have recently suggested that the picture is more complex in the Weddell Sea, where the heavy snow layer encourages superimposed ice formation as well as the occurrence of liquid gap layers at the snow-ice interface. Superimposed ice is formed by snow surface melting, percolation, and refreezing on the top of the ice [*Gerland et al.*, 1999].

1.3. Modeling Heat Transfer and Salinity Variations in Sea Ice

[10] First attempts in modeling the sea ice vertical heat transfer and storage and mass balance were made in the 1970s [*Maykut and Untersteiner*, 1971; *Semtner*, 1976]. Recently, improvements in the representation of thermodynamic processes in sea ice models [*Bitz and Lipscomb*, 1999; *Taylor and Feltham*, 2004; *Huwald et al.*, 2005a; *Notz*, 2005] have been motivated by the importance of sea ice on high latitude climates, which themselves have a prominent role in the global climate system. Currently, most climate models include at least a sea ice thermodynamic component, such as the one of *Semtner* [1976] or the more recent one of *Bitz and Lipscomb* [1999] simulating sea ice temperature profile and thickness as main prognostic variables. Only the latter has salinity-dependent thermal properties but hold the vertical sea ice salinity profile fixed in time. To correct this has frequently been reported as a next important step in their development [*Leppäranta*, 1993; *Bitz and Lipscomb*, 1999; *Eicken*, 2003].

[11] Modeling the temporal evolution of the sea ice salinity profile has been approached several times. *Untersteiner* [1968] theoretically tried to find which brine drainage mechanism was most responsible for the characteristic shape of the equilibrium MY salinity profile in the Arctic [see, e.g., *Schwarzacher*, 1959]. He suggested that intense summer desalination induced by downward percolation of surface meltwater through the permeable ice cover, what he called flushing, was the likely best candidate.

[12] A numerical model of winter desalination of FY sea ice was developed by *Cox and Weeks* [1988] (hereafter referred to as CW88), based on laboratory observations of *Cox and Weeks* [1975]. It relies on parameterizations of salt entrapment during ice growth, and desalination by gravity drainage and brine expulsion. The simulated salinity profiles looked roughly in agreement with current knowledge. Nevertheless, an attempt by *Cox* [1990] to validate the model against Arctic observations was unsuccessful. The modeled desalination rates were too strong and an improbable suction of salt had to be added to gain a better agreement with observations. In contrast to Cox's study, *Eicken* [1992] tested the CW88 model for sea ice in the Weddell Sea and successfully compared the simulated profiles to the observed ones. The agreement was independent of the growth mechanism (i.e., congelation or frazil), and the date of ice growth onset was found to be of primary importance. In a study of Ross Sea ice using the CW88 model, *Maksym and Jeffries* [2000] needed to add the

impact of seawater flooding during snow-ice formation to have reasonable agreement with observations.

[13] The CW88 model only applies to non flushing situations. Until now, no parameterization of the flushing mechanism has been proposed. Thus previous sea ice salinity models could not simulate a complete seasonal cycle of the ice salinity in the Arctic. In addition, there is no coupling between salinity and temperature in the CW88 model (i.e., the sea ice thermal properties do not depend on salinity and temperature). Furthermore, in the CW88 model, the ice desalination rates have empirical, prescribed functional dependence on model diagnostics (e.g., vertical temperature gradient or temperature temporal derivative). These functions derive from data taken in cold room experiments by *Cox and Weeks* [1975].

[14] Recently, it has been proposed to apply mushy layer theory to sea ice. It provides an integrated approach of modeling sea ice halothermodynamics [*Worster and Wettlaufer*, 1997]. "Mushy layer" is a metallurgic term standing for two-phase, two-component reactive porous medium. The mushy layer equations include the conservations of heat, brine salinity and momentum. A coupling term between fluid and heat transport is included. The bulk sea ice thermal properties are weighted means of the respective contributions from the solid and liquid phases. Within the mushy layer framework, *Taylor and Feltham* [2004] solved the heat conservation equation. In their study, the salinity profile was constant in space and time and the vertical fluid transport was prescribed. Therefore, in practice, inside the ice, their thermodynamical approach was equivalent to *Bitz and Lipscomb* [1999]. However, since their purpose was to model the evolution of melt pond depth on sea ice at Surface Heat Budget of the Arctic ocean (SHEBA), their model also included sophisticated surface meltwater and radiative transfer components. *Notz* [2005], with an enthalpy-based approach, has modeled both heat and salt conservation equations, but so far limited his application to very few test cases.

1.4. Goals of This Study

[15] This paper addresses the following questions. (1) How does the vertical desalination proceed in undeformed Arctic sea ice, especially in summer? (2) Is it possible to reproduce the temporal evolution of salinity by using a sea ice model of reasonable complexity? What degree of accuracy can we expect from this type of model? (3) What are the physical processes and interactions between heat transfer, brine volume and desalination described by the model? (4) Can modeling help us infer the actual contribution of surface meltwater to desalination by downward percolation in undeformed bare ice?

[16] In order to answer those questions, we first analyze a series of salinity profiles observed in 87 fast ice cores from the Point Barrow area, near the north coast of Alaska (section 2). We compare uncertainty due to errors to extraction and horizontal variability. The fast ice has the advantage of being driven mostly by thermodynamic processes.

[17] Then, we propose a new, semiempirical one-dimensional halothermodynamic sea ice model (section 3). The thermodynamic component [*Bitz and Lipscomb*, 1999] accounts for the effect of the salinity profile on heat transfer and storage. The halodynamic component (i.e., computing the ice salinity profile) is an extended version of the CW88 model. We add to CW88 a formulation of flushing so that the model is able to work over a complete seasonal cycle. The model components are coupled through a brine volume function of salinity and temperature. Over a 5% brine volume threshold, the brine network connects and sea ice is permeable to fluid transport. Our model includes several aspects of mushy layer physics. We chose the thermodynamic model to have a simplified representation of snow physics (single layer, no salinity, no penetration of shortwave radiation through) in order to reduce the number of complex processes in the model.

[18] Next, the model is run under Point Barrow conditions (section 4). We first try to match observed and modeled ice and snow mass balance (section 4.1). *Huwald et al.* [2005b] have shown an accurate mass balance comparison between model results and observations is thwarted by high variability at small horizontal scales in snow depth and ice thickness. In addition, desalination by flushing depends sensitively on the ice melt onset date. Keeping this in mind and the fact that the observations we use for atmospheric forcing and the initial conditions of the ice salinity profile, ice thickness and snow depth were not made at the exact same site, we emphasize the strength of this study is in exploring the salinity model (sections 4.2 and 4.3) and its sensitivity to snow physics (section 4.4) and internal parameters (section 4.5) rather than attempting to simulate the mass balance. Also, we trace the summer freshwater pathways in the model and compare it to existing observations (section 5). Then we discuss our results and sum up the conclusions of our study (section 6). In a companion manuscript [*Vancoppenolle et al.*, 2006], we study the implications of the time-dependent ice salinity in large-scale ice mass balance simulations.

2. Observation of Fast Ice Desalination at Point Barrow, Alaska

[19] The salinity and mass balance data we use in this study (D. K. Perovich et al., Arctic coastal processes data report 2001, 2001, available at http://www.arcticice.org) come from two seasons of yearlong observations (1999–2000 and 2000–2001) of FY landfast sea ice at two different sites close to Point Barrow, on the Alaskan North Coast: Chukchi Sea (CS) and Elson Lagoon (EL) (Figure 1). The combination of seasons and data sets correspond to four subsets, which we refer to as CS2000, CS2001, EL2000, and EL2001.

[20] The ice from the two sites exhibit some differences. CS is an open site where the wind tends to blow away most of the snow, while EL is more inland, with a local wind pattern tending to trap snow. Thus snow is deeper at EL than at CS. The ice tends to form significantly earlier at the EL site, but the maximum thickness is smaller than in the CS site since the deep snow reduces ice growth rates at EL. The ice at EL is overall slightly more saline than in CS since the water from which ice forms is more saline at EL (H. Eicken, personal communication, 2006). The ice at EL is often highly sediment laden, which is rarely the case at the CS site [*Frey et al.*, 2001; *Stierle and Eicken*, 2002].

[21] The two studied seasons are also different. Their winter temperatures (from the Point Barrow meteorological

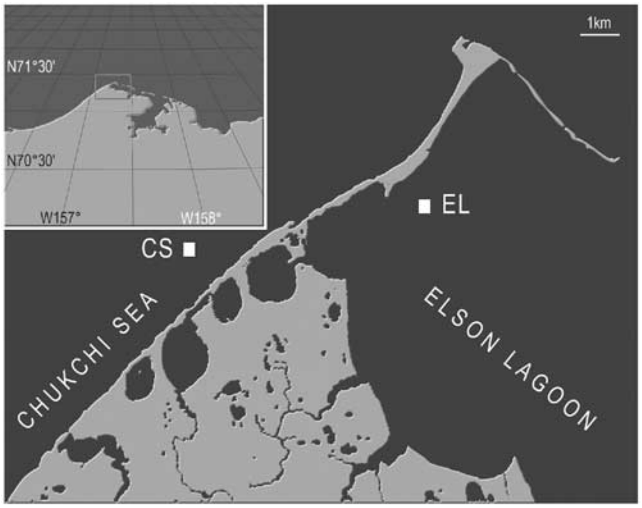

Figure 1. Map of Point Barrow neighborhood. Both sampling sites are indicated: Chukchi Sea (CS) and Elson Lagoon (EL).

station) are similar, but spring and summer were warmer in 2000 than in 2001 (Figure 2). The average 2 m air temperature in May 2000 (2001) was −10.7°C (−14.3°C), and in June it was 2.6°C (1.7°C). The surface melt appears discontinuous during early summer, with temperature being alternatively above (from 0 to 15°C) and below (between −3 and −1°C) the freezing point (period around 5 days). Superimposed ice was observed to form at the CS site in 2000, but not in 2001, which is coherent with much thicker snow in 2000 than in 2001 [*Eicken et al.*, 2002, 2004; D. K. Perovich et al., Arctic coastal processes data report 2001, 2001, available at http://www.arcticice.org]. We also suspect some superimposed ice formation in EL in late winter/early summer 2000 and 2001, since the snow was thicker than 30 cm both years, but no clear mention of superimposed ice was made in the data record.

2.1. Mass Balance

[22] Ice/snow mass balance was monitored at both sites and is presented in Table 1. The instrumentation at the sites typically consisted of a data logger, snow stakes, thickness gauges and an above ice acoustic sounder measuring the height above sea level every hour to within 5 mm. A thermistor string measured vertical profiles of temperature. The thickness gauges consisted of an ablation stake measuring mass loss at the surface and a hot wire gauge measuring bottom accretion or ablation. Data was manually collected every 1–2 weeks during winter and every 2–4 days during the melt season. Four stake and gauge combinations were installed at each site. Accuracies of stake and gauge readings were about 0.5 cm. EL ice typically forms earlier and has more snow. Since deeper snow takes longer to melt, the onset of sea ice surface melt occurs later at EL.

2.2. Salinity Profiles

[23] Ice salinity profiles were measured from ice cores. The number of cores and their origin is detailed in Table 2. Pond ice samples were only taken at the CS site in 2000 (7 cores). Salinity was measured every 5 cm within a core, and cores were taken every 2 days in summer. In summer, the cores were mostly confined to the upper 50 cm of ice.

2.2.1. Extraction Errors

[24] The ice coring approach is known to underestimate salinity since brine drains during core extraction, especially in the lower (warm) parts of the cores [*Notz et al.*, 2005], and in high salinity core sections [*Eicken et al.*, 1991]. In summer, when the ice is warmer, the brine loss is potentially higher. In winter, when the ice is cold, the error in salinity due to extraction should be of a few tenths of permils at most (<0.2‰ for ice salinities around 5‰). However, near the bottom, the ice is always relatively warm and can easily have a loss in brine salinity of more than 1‰. On the other extreme, in summer, when the ice is warm, the loss of brine can be substantial and depends on how quickly the core is processed after extraction. For high salinities (>5‰), the brine loss may be as high as 0.5 to 1‰. However, for warm, low-salinity ice, the impact of brine loss on salinity will not be as high (e.g., around 0.2‰ for a 1‰ salinity). In both cases, the salinity deficit due to brine loss represents from 10 to 20% of the initial salinity.

2.2.2. Horizontal Variability

[25] We briefly describe the local horizontal variability of the salinity profiles as an estimate of their uncertainty. The discrete nature of brine drainage channels is a source of horizontal variability below about 10 cm [*Cottier et al.*, 1999]. This variability is overcome by the core diameter (10 cm). Larger-scale variability, at 2–20 m scale, is controlled by variability in brine drainage [*Tucker et al.*, 1984; *Eicken et al.*, 1991].

[26] In the year 2001, a few synchronous salinity profiles were measured at 10-m intervals at both sites in late winter and early summer. The mean and standard deviation of the intrasite bulk salinities for each time period is given in Table 3. The bulk salinities reported in early summer are only for the top 50 cm due to brine drainage difficulties in the lower parts of the cores. The standard deviation of the intrasite bulk salinity ranges from 0.22–0.28‰ in late winter and 0.05–0.44‰ in summer.

[27] Naturally the salinity at a particular depth varies more than the bulk salinity across the ice cores. Figure 3 illustrates the depth-dependent variations in salinity. The late winter cores have a characteristic C shape, as described

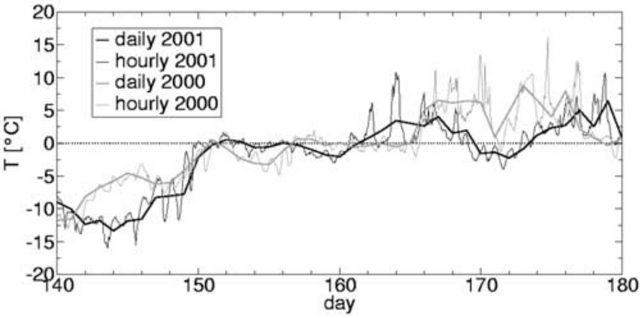

Figure 2. Summer evolution of 2 m air temperature in 2000 and 2001 according to meteorological station data. The date 1 June is day 153 (152) in 2000 (2001).

Table 1. Observed Mass Balance

	Chukchi Sea		Elson Lagoon	
	1999–2000	2000–2001	1999–2000	2000–2001
Initial ice thickness, cm	37	22	54	30
Initial snow thickness, cm	3	3	3	3
First observation date	12 Nov 1999	2 Nov 1999	10 Nov 2000	3 Nov 2000
Maximum ice thickness, cm	154.3	162.8	148.6	157.8
Maximum snow thickness, cm	36	11	47.8	30.1
Maximum snow thickness date	18 May	21 May	26 May	18 May
Ice surface melt initial date	14 Jun	4 Jun	?	14 Jun
Bottom melt initial date	23 Jun	4 Jun	13 Jun	21 Jun

in section 1.2, with variations in the overall amplitude of bulk ice salinity that depend mostly on the thickness. When profiles are normalized by dividing the vertical coordinate by the core length, as shown in Figure 3, the standard deviation for a 5-cm layer at a given normalized depth is on average 0.76‰ at CS and 0.88‰ at EL in late winter.

[28] In early summer, rapid desalination at melt onset adds to the difficulty of estimating the horizontal variability in the salinity profiles. We compare cores taken at most 2 days apart, but it is still possible that our horizontal estimates are made somewhat larger by temporal variability as well and hence are more conservative. The standard deviation for a 5-cm layer at a given normalized depth is on average 0.34‰ in summer, which is comparable to the standard deviation of the bulk salinity for the whole 50-cm layer.

[29] In summary, we consider that the average error due to horizontal variability in bulk salinity is 0.25 (0.30) ‰ in winter (summer) and that the error at a particular depth is 0.82 (0.34) ‰ in winter (summer). In late winter, the uncertainty due to horizontal variability exceeds the error due to brine loss upon extraction, except near the bottom where the extraction error is considerable. In early summer, these two sources of error are comparable in the upper 50 cm, and we expect the extraction error dominates below this layer.

2.2.3. Summer Desalination Sequences

[30] There are a sufficient number of salinity profiles to visualize bare ice desalination sequences for CS2000, CS2001, and EL2001. Furthermore, for CS2000, we also have 7 salinity profiles of ponded ice, so we can contrast salinity in bare ice and ponded ice.

[31] In summer 2000 at the CS site, the average salinity of bare ice (3.38 ± 0.65‰) was significantly higher than the salinity of ponded ice (2.50 ± 0.55‰). The shapes of the profiles were also different (Figure 4). In bare ice, the typical more or less linear profile with low surface salinity is well established (i.e., the bulk salinity of the uppermost 50 cm of ice is under 3‰) after 11 days of surface melt, if we assume that surface melt started on 1 June (see Figure 2). On 15 June though, a special event increased the surface salinity by 2‰. This event could be due to lateral or vertical intrusions of salty water from various origins (seawater flooding, lateral drainage of brine). After this event, progressive desalination was typical again. In ponded ice, the desalination sequence is mostly continuous and the ice reaches a roughly vertically constant profile, with a salinity slightly above 2‰ on 23 June.

[32] In 2001, the bare ice desalination sequences observed at CS (7 profiles, Figure 5a) and EL (6 profiles, Figure 5b) sites show progressive, practically monotonic, desalination patterns, with no apparent seawater flooding as in 2000. Unfortunately, the first core at CS was taken on 2 June, after the onset of flushing. At EL, the rapid desalination started between 1 and 5 June. At both sites (particularly visibly at EL), we can see the ice salinity profile rapidly switch from a C-shaped to a more or less linear one with low surface salinity. After 13 (12) days of surface melt at CS (EL), considering that surface melt started on 1 June (see Figure 2), the uppermost 50 cm of ice had a salinity under 3‰.

3. The Model

[33] The model we use in this study is a semiempirical one-dimensional model of undeformed, bare (i.e., unponded), Arctic sea ice, resulting from the coupling of thermodynamic and halodynamic components. We are currently working on the model to extend it to Antarctic situations. The thermodynamic component computes heat transfer and storage (i.e., temperature profile) as well as ice thickness and snow depth. The halodynamic component resolves brine entrapment and drainage mechanisms, which

Table 2. Ice Core Data[a]

		Number of Cores			Bulk Salinity, ‰		
Period	Site	Total	Summer	Summer Bare Ice	Winter	Summer	Comments
1999–2000	CS	29	18	11	5.34	3.53	superimposed ice widespread in summer
	EL	9	3	3	5.69	3.02	surface layers highly sedimented
2000–2001	CS	17	9	9	5.69	3.89	surface impervious after 2 weeks of melt
	EL	13	6	6	5.73	3.52	sediments/suspected superimposed ice formation
		68	36	29	5.61	3.49	total number of cores, mean salinity

[a] In summer, core length is often 50 cm.

Table 3. Horizontal Variability of Ice Bulk Salinity, 2001[a]

	Winter-Spring						
	12 Mar Core 1	12 Mar Core 2	3 May	4 May Core 1	4 May Core 2	Mean	σ
Chukchi Sea							
Core length, m	1.13	1.29	1.40	1.54	1.45	1.36	0.14
Mean salinity, ‰	5.17	5.47	5.04	5.64	5.50	5.36	0.22
	11 Mar	14 Mar	1 May	5 May		Mean	σ
Elson Lagoon							
Core length, m	1.11	1.13	1.26	1.42		1.23	0.12
Mean salinity, ‰	5.99	5.49	5.22	5.48		5.55	0.28
	Early Summer						
	7 Jun	9 Jun	9 Jun			Mean	σ
Chukchi Sea							
Core length, m	0.50	0.50	1.46			0.82	0.45
Mean salinity (upper 50 cm), ‰	3.36	2.29	2.97			2.87	0.44
	8 Jun	9 Jun				Mean	σ
Elson Lagoon							
Core length, m	0.45	1.38				0.92	0.47
Mean salinity (upper 50 cm), ‰	3.20	3.29				3.25	0.05

[a] The σ refers to the intercore standard deviation. The single-core mean salinities are weighted according to the length of each core section. The intercore means are arithmetic means, computed independently of core length.

lead to the computation of the vertical salinity profile. In addition, the haline component treats meltwater flushing, but the thermodynamic component ignores meltwater thermal effects like ponding and refreezing.

3.1. Thermodynamic Component

[34] The thermodynamic sea ice model used here is the one-dimensional energy-conserving model of *Bitz and Lipscomb* [1999]. Model prognostic variables are the ice thickness h_i, the snow depth h_s, the vertical temperature profile $T(z,t)$ in the ice-snow system and the surface temperature $T_{su}(t)$, where t is the time and z is the vertical coordinate. $T(z,t)$ is computed by numerically solving the heat diffusion equation. $T_{su}(t)$ and the growth/melt rates dh_x/dt (where suffix x refers either to snow or ice) are deduced from the heat balance between inner conduction fluxes and atmospheric (respectively oceanic) external fluxes at the upper (respectively lower) interfaces. The thermodynamic effect of salinity, and its control on the size of brine pockets, is represented by the functional dependence of the thermal properties on salinity and temperature (which affect heat diffusion and growth/melt rates). The atmospheric fluxes include radiative shortwave (SW), radiative longwave (LW), and turbulent sensible and latent heat components.

[35] The ice cover is represented with one layer of snow on top of N layers of sea ice. The snow layer has a temperature T_s and each layer (l = 1, . . ., N) of sea ice has a specific temperature T_i^l and salinity S_i^l (see Figure 6).

[36] The theoretical basis of this model relies on two assumptions involving model state variables, the temperature T and the salinity S. (1) The approximate freezing temperature of a saline solution, T_f (in °C), is a linear function of its salinity S given by

$$T_f = -\mu S, \tag{1}$$

where μ = 0.054°C^{-1}, as determined by *Assur* [1958]. (2) The brine pockets are in local thermal equilibrium with the surrounding ice and permanently at their freezing temperature, so that they adapt their salinity σ by changing size to the local ice temperature:

$$T = -\mu\sigma. \tag{2}$$

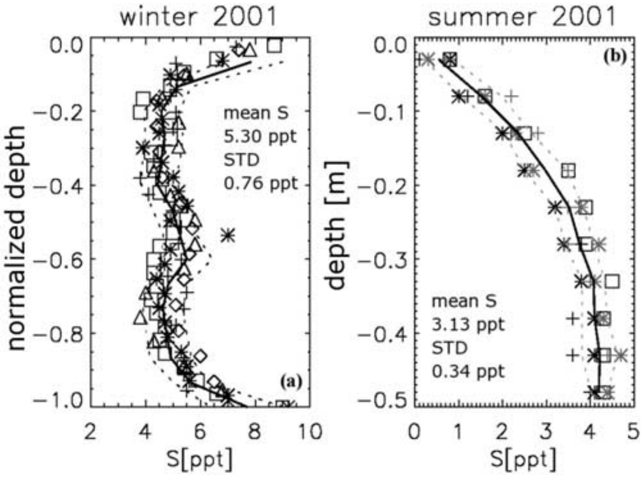

Figure 3. Horizontal variability of vertical salinity profile, 2001. (a) CS, winter, normalized profiles: 12 March, two nearby profiles (crosses, stars); 3 May (squares); 4 May, two nearby profiles (triangles, diamonds). (b) CS and EL, early summer, profiles restricted to upper 50 cm. CS (black symbols): 7 June (squares); 9 June, 2 nearby profiles. EL (grey symbols): 8 June (crosses), 9 June (stars). On both panels, the mean profile (solid line) and the one standard deviation range (dotted lines) are shown. Note the difference in vertical axes. The profiles shown here correspond to some of the profiles of Table 3. Nearby profiles are associated to cores extracted at 10-m intervals.

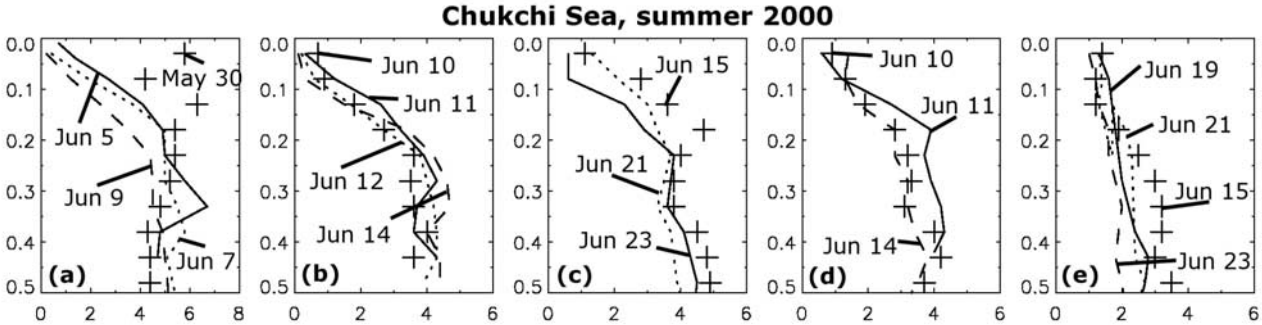

Figure 4. Chukchi Sea site, summer 2000. Observed surface desalination sequence during the early melt period for (a–c) bare ice and (d–e) ponded ice. Horizontal and vertical axis refer to salinity [‰] and depth [m], respectively.

In this context, σ is the salinity of the brine pockets, while S is the salinity of the ice if brine were distributed uniformly throughout the ice. Thus σ and S are related to each other by

$$\sigma e = S. \tag{3}$$

The relative volume of brine inclusions e (dimensionless, hereafter referred to as brine volume) is consequently only a function of S and T [*Schwerdtfeger*, 1963]:

$$e = -\mu \frac{S}{T}. \tag{4}$$

[37] The brine density ρ_b is given from *Zubov* [1945] by assuming a linear dependence on brine salinity,

$$\rho_b = \rho_w(1 + c\sigma), \tag{5}$$

where ρ_w = 1000 kg m^{-3} is the fresh water density and c = 0.8 × 10^{-3} ‰$^{-1}$ is an empirical coefficient.

[38] The mathematical formulation of the thermal properties of the ice relies on the brine volume. First, the specific heat, $c(S,T)$, describes the magnitude of heat storage in the ice. It is given according to *Malmgren* [1927] and *Ono* [1967], and can at warm temperatures be 2 orders of magnitude larger than its asymptotic limit for cold ice. Second, the thermal conductivity, $k(S,T)$, regulating the internal heat transfer, is specified according to *Untersteiner* [1964]; $k(S,T)$ is decreased at most by 20% at warm temperature. The third S-T-dependent thermal property is the sea ice energy of melting $q(S,T)$, defined as the energy required to melt a unit volume of sea ice of salinity S and temperature T. It modulates the growth/melt rate of sea ice at its interfaces with atmosphere and ocean. It is significantly lower than the standard latent heat of fusion of pure freshwater ice, because it takes into account the internal melt.

[39] The radiation scheme assumes that a fraction i_o of the incoming net solar radiation does not contribute to the surface energy balance and penetrates inside the snow/ice system and is absorbed and transmitted according to Beer's law.

[40] The simplification of snow physics is certainly one of the limits of the model. Snow cover is highly complex. Its depth and properties are highly variable on small horizontal scale [*Sturm et al.*, 2002], even on the same floe. Since snow is not the main focus of the paper, we only use one layer of snow, with no penetration of solar radiation, as in, for example *Maykut and Untersteiner* [1971], or more recently *Taylor and Feltham* [2004]. The snow is assume to be of zero salinity, though it was observed to be slightly saline (especially in the lower layers) in landfast FY ice of the Canadian Archipelago [*Mundy et al.*, 2005]. Snow compaction and meltwater refreezing are also neglected.

3.2. Halodynamic Component

[41] The halodynamic component of the model computes the temporal evolution of the vertical salinity profile $S(z,t)$. Experiments performed in the sixties and the seventies (see *Weeks and Ackley* [1986] for a review) led *Untersteiner* [1968] and CW88 to formulate the changes in the salinity profile $S(z,T)$ by

$$\frac{dS}{dt} = \left.\frac{dS}{dt}\right|_{\exp} + \left.\frac{dS}{dt}\right|_{gd} + \left.\frac{dS}{dt}\right|_{flu}. \tag{6}$$

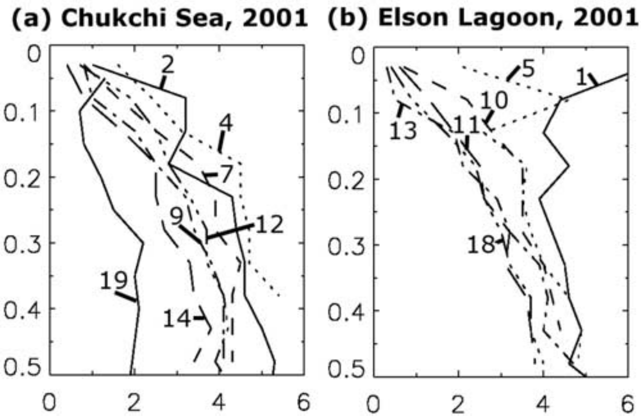

Figure 5. Desalination sequences at (a) Chukchi Sea and (b) Elson Lagoon sites during the early melt period, 2001. The numbers correspond to the days of June. Horizontal and vertical axis refer to salinity [‰] and depth [m], respectively.

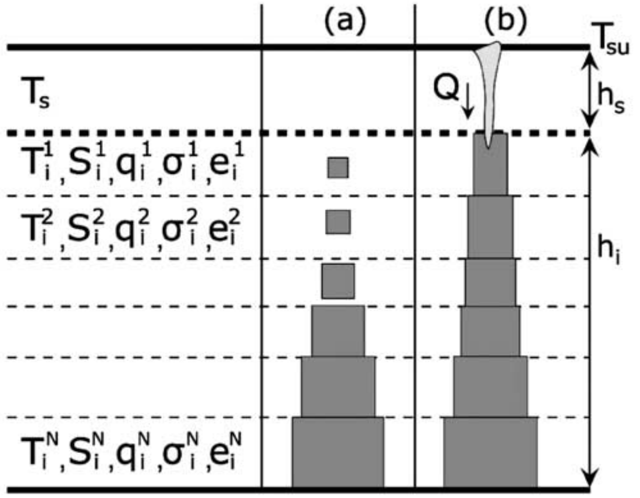

Figure 6. Vertical grid of the sea ice when snow is present. Typical brine network configuration in (a) winter and (b) summer. All symbols are defined in the text in section 3.

The different terms on the right hand side correspond to brine expulsion, gravity drainage and flushing. The bottom boundary condition depends on how salt is trapped in the ice during growth and is done as in CW88: each new layer formed at the bottom of sea ice has a salinity given by the multiplication of the fractionation coefficient f by the salinity of the underlying ocean S_w. The more rapid the ice growth, the more salt trapped inside the ice. New sea ice is assumed to form at the seawater freezing point ($T_b = -\mu S_w$). Thus the initial brine volume of new ice is $e_b = f$. For the first two tendency terms of the salinity equation, we use slightly modified versions of CW88 equations. For the flushing term, we propose a new formulation.

3.2.1. Brine Expulsion

[42] When a brine pocket cools, the thermal contraction of the ice around the pocket is greater than that of the liquid inside, producing a pressure gradient that may lead the pocket wall to rupture. Actual observations of brine expulsion are still lacking, so that the direction of the expulsion flow is not well known, although indications of both downward and upward flow are suggested [*Cox and Weeks*, 1975; *Cottier et al.*, 1999]. Saline snow [*Mundy et al.*, 2005] and the presence of highly saline frost flowers on top of new ice [*Martin et al.* 1995] also support the upward migration of brine in sea ice. Nevertheless, the mechanism through which this happens is not yet clear.

[43] Through volume conservation arguments, *Cox and Weeks* [1986] provide an expression for the subsequent expulsion desalination rate of a piece of ice of uniform temperature. The expulsion rate is specified as a function of the cooling rate through temperature-dependent formulas of brine density $\rho_b(T)$ and salinity $\sigma_b(T)$. For each layer, we assume local equilibrium and use the functional expression E of Cox and Weeks:

$$\left.\frac{dS}{dt}\right|_{\exp} = E\left[\frac{dT}{dt}\right], \tag{7}$$

though with different formulas (equations (4) and (5)) for $\rho_b(T)$ and $\sigma(T)$, to be consistent with our thermodynamic model component. The impact of this difference on the model results is not significant, since the magnitude of this process proves to be very small. The temperature tendency (dT/dt) is computed by the thermodynamic component. Compared to CW88, we assume that the brine is not expelled outside the ice. Instead, we assume that the brine is transported equally upward and downward, with a barrier to flow at the upper surface and free passage into the ocean beneath. This is motivated by the fact that brine expulsion leads more to a redistribution than to a net loss of salt in the ice [*Notz*, 2005].

3.2.2. Gravity Drainage

[44] Gravity drainage, the main reason for early winter desalination rates, gathers all processes where brine is expelled from the ice under the influence of gravity through an interconnected brine network [*Weeks and Ackley*, 1986].

[45] The actual mechanism beyond gravity drainage is not clear. First, ice growth-driven gravity drainage was proposed by *Untersteiner* [1968] and *Cox and Weeks* [1975]. The upward advection of ice layers driven by ice growth transports brine above sea level and creates a pressure head having the potential of expelling the brine out of the ice. The second suggested mechanism is a temperature-driven gravity drainage. In winter, the ice is the warmest at its base, which creates an unstable brine density profile. If the ice is porous enough, convection ensues, causing net downward salt transport and a local decrease in salinity. Similarly, the downward temperature-induced brine salinity gradient induces molecular diffusion of salt inside the permeable region. If the brine tubes are thin enough, the capillarity forces are strong enough to compensate the destabilizing buoyancy forces, as suggested by the data from *Mercier et al.* [2005].

[46] *Cox and Weeks* [1975] indirectly observed gravity drainage as a residual between observed desalination rates and computed brine expulsion. Then, CW88 devised an empirical regression formula linking the desalination rate, brine volume e and temperature T gradient. As in CW88, we assume that gravity drainage depends on the temperature gradient and brine volume. If $\partial T/\partial z < 0$ and $e > 5\%$, the desalination rate is

$$\left.\frac{\partial S}{\partial t}\right|_{gd} = \delta(1 - \eta e)\frac{\partial T}{\partial z}, \tag{8}$$

and 0 otherwise. δ and η are empirical coefficients. δ controls the magnitude of the desalination flow. Contrary to CW88 who proposed to use $\delta_{lab} = 1.68 \times 10^{-7}$ °C^{-1}m s^{-1}, based on lab observations, we recommend to use $\delta_{mod} = 5.88 \times 10^{-8}$ °C^{-1}m s^{-1} (suitable for our modeling study), which is 65% smaller than their value, for reasons we explain in section 4.2. The value $\eta = 20$ reflects the fact that gravity drainage is 0 for $e = 5\%$ and then its intensity increases (i.e., $\partial S/\partial t|_{gd}$ decreases toward more negative values) for greater brine volumes. We allow no gravity drainage for any layer above an impermeable layer. Since (8) implicitly assumes vertical brine flow, it is mass conserving. In other words, the downwelling salt flux from each layer is implicitly transported to the underlying layer.

3.2.3. Flushing

[47] Flushing is a special kind of gravity drainage, where the pressure head and water are provided by the fresh surface meltwater going through the permeable summer brine network. First mentioned by *Untersteiner* [1968], it is believed to strongly contribute to the summer surface desalination of pack ice and to be responsible for the shape of the MY salinity profile, important for sea ice surface melt rate and equilibrium thickness [*Vancoppenolle et al.*, 2005]. The picture is actually more complex than a simple one-dimensional vertical downward meltwater flow, as shown by observations of summer ice hydrology at SHEBA and later at Point Barrow by *Eicken et al.* [2002]. Lateral meltwater flow directed toward the lowest topographic features was found to be highly significant, and even dominant during the early stages of surface melt. Our model only considers the vertical component of the meltwater flow through bare ice.

[48] Field experiments by *Eicken et al.* [2002] suggest that once a permeability threshold is reached (i.e., when brine channels can be assumed to be connected), any available meltwater is almost instantly transferred through the ice matrix. The summer production of meltwater at the ice surface is around 10^{-4} kg m^{-2} s^{-1} while the flow the ice can sustain once permeable is much higher and therefore flushing can be seen as instantaneous. We thus make the following hypothesis: Brine drainage processes are much more rapid than the thermal reequilibrium processes. This prevents the brine channels from enlarging through advection of heat by meltwater.

[49] Once the permeability threshold is reached ($e_T = 5\%$, mentioned both by theoretical [*Golden et al.*, 1998] and experimental studies [*Eicken et al.*, 2004] and the surface is melting ($T_{su} \geq 0°C$), we assume that flushing occurs. A fraction of the meltwater flows through the brine channels, replacing salty brine by almost fresh meltwater coming from the top of the ice. If these requirements are not fulfilled, the meltwater is assumed to contribute to lateral drainage to ocean through cracks and leads, or to collect in the lowest gravity areas and form melt ponds, as recently observed by *Eicken et al.* [2002].

[50] The ice salinity profile is converted into the vertical profile of brine salinity, using equation (3), and brine volume, using equation (4). The meltwater mass flow Q per unit area of sea ice [kg m^{-2} s^{-1}] through the ice matrix is then

$$Q = \phi \rho_x \left. \frac{dh_x}{dt} \right|_{su}, \tag{9}$$

if $e \geq e_T = 5\%$ and is set to zero otherwise. The subscript x refers to either snow or ice. ρ_x is the density of ice/snow and $dh_x/dt|_{su}$ is the surface melt rate computed by the thermodynamic component; ϕ is the prescribed fraction of the meltwater allowed to percolate vertically through the ice matrix. The salinity of this meltwater mass is $S_Q = 0‰$ if meltwater comes from snowmelt and $S_Q = S_i^1$ if the ice surface is melting.

[51] During flushing, Q penetrates the brine network and pushes brine downward. To compute the new brine salinities after flushing, we solve the brine mass conservation equation:

$$\frac{\partial \sigma}{\partial t} = -\frac{Q}{e\rho_b} \frac{\partial \sigma}{\partial z}. \tag{10}$$

We assume that the mass flow is the same through all horizontal brine network sections and that the brine volume is fixed during the process. Once σ is computed, we recompute S, using equation (4).

[52] The variable ϕ, the meltwater partitioning coefficient and e_T, the brine volume permeability threshold, dominate this parameterization; ϕ controls the impact of the desalination flow on salinity, while e_T controls the flushing onset date. i_0 is an important indirect parameter, since it controls the penetration of net SW radiation to the ice interior, which can connect the brine pockets.

[53] We numerically solve equation (10) with an implicit scheme, which is unconditionally stable. At each time step, the vertical grid is recomputed to adapt to the new ice thickness. We linearly redistribute the mass of salt and heat content onto the new grid.

[54] At this time our model only attempts to represent the summer melt water pathways and storage in sea ice for an unponded slab of sea ice. *Taylor and Feltham* [2004] have developed a model of melt pond evolution in sea ice, but prescribed the vertical flow of meltwater through the ice in summer. Our respective approaches could be complementary in a two-cell model with cells of bare and ponded ice connected by a freshwater flux proportional to $(1-\phi)$. Furthermore, an account for snow-ice formation would also make our model more general. Specifying the exact source of flooding seawater during such events might be difficult though, since seawater pathways in sea ice are not well understood. The study of *Maksym and Jeffries* [2000] indicates that the flooding of the bottommost snow layers during snow-ice formation events is probably not performed by upward percolation of seawater through a permeable brine network. Nevertheless, other potential pathways for seawater to flood the ice, as lateral floe borders, or wider vertical channels (as cracks or large moats) are not, to our knowledge, well documented.

3.2.4. Forcing and Experimental Design

[55] We made three control experiments, corresponding to conditions at CS in 1999–2000 (CS2000-1) and 2000–2001 (CS2001-1) as well as at EL in 2000–2001 (EL2001-1). The model is initialized with observed values of ice thickness and snow depth, temperature and salinity profiles. The objective while setting the experimental design was to calibrate the snow/ice mass balance in order to provide a suitable background to compare the model and observed ice desalination.

[56] It is considered that the mass balance and salinity data have a spatial horizontal scale on the order of the floe size, since (1) four gauges and stakes were used at each site and (2) spatial variability in ice salinity was assessed. The most important sources of forcing variations at scales comparable to the floe size come from variability in clouds, in snow depth and in seawater state (due to local geographic and bathymetric features) for which we do not have enough or any data. Therefore some tuning was required to adjust

the snowfall rate, the downwelling LW radiation and the oceanic heat flux.

[57] We force the model with a hybrid transient and climatological forcing. For temperature, pressure and wind speed, we take daily averages of hourly observations made at the meteorological station at Point Barrow, provided by the Climate Monitoring and Diagnostics Laboratory (CMDL) Web site (http://www.cmdl.noaa.gov/infodata/ftpdata.html). Cloudiness and relative humidity come from daily interpolations of widely used monthly climatologies [*Berliand and Strokina*, 1980; *Trenberth et al.*, 1989].

[58] The incoming SW radiation flux is prescribed as a function of latitude, cloudiness and humidity [*Zillmann*, 1972]. The incoming LW radiative flux is parameterized according to *Berliand and Berliand* [1952] as a function of air temperature, cloudiness and specific humidity. Mass balance simulations show that the incoming LW is the most likely forcing component to be underestimated. The cloudiness climatology we use is a source of error to which the LW flux is especially sensitive at high temperatures. Since *Lindsay* [1998] mention that errors in the incoming LW flux with such parameterizations can be as large as 20 W m^{-2}, taking into account uncertainties linked to clouds, we increased the LW radiation by 10% to bring the melt onset date to the observed value. The turbulent sensible and latent heat fluxes are computed with bulk aerodynamic formulas described by *Goosse* [1997].

[59] Since snow depth is highly variable even at subkilometer scales [*Sturm et al.*, 2002], we derived 3 specific snow precipitation temporal data sets, one for each case study, from the snow depth temporal evolution data. We interpolated the change in snow depth on a daily time step to infer daily snowfall values. If snow depth happened to decrease, then the precipitation rate was set to 0. In other words, we specify depth when snow accumulates but let snow melt in the model.

[60] The oceanic heat flux F_w is empirically calibrated to improve the agreement between observed and model snow/ice mass balance. At CS (EL), a value of $F_w = 4.5$ (3.0) W m^{-2} is used. These values lie in the range proposed by *Krishfield and Perovich* [2005]. The difference in the F_w optimal values between the two sites suggests that their geographical configuration (CS, open sea; EL, lagoon) affects heat transfer between seawater and ice.

[61] Observations by *Eicken et al.* [2004], made at the same site during similar field campaigns, suggest albedo values of 0.80, 0.65 and 0.50 for dry snow, melting snow, and bare ice, respectively. The fraction of net solar radiation penetrating below the surface i_0 is taken to be 0 in the presence of snow and 0.30 without snow, an average of *Grenfell and Maykut* [1977] values. i_0 is a key parameter since it controls the amount of internal warming, especially in the upper layers of the ice (where flushing occurs) and also the increase in brine volume. Thermal conductivity of the snow is set to $k_s = 0.31$ W m^{-2}, snow density to $\rho_s =$ 330 kg m^{-3}. $N = 20$ layers in the ice and a time step of $\Delta t =$ 1 day are used.

4. Model Results

[62] In this section, we first examine the modeled snow/ice mass balance (section 4.1). Second, we analyze the model desalination in detail for winter (section 4.2) and summer (section 4.3). Finally, the sensitivity of the salt and mass balance to the model representation of the snow (section 4.4) and to the main parameters of the flushing parameterization (section 4.5) is studied.

4.1. Mass Balance

[63] Figure 7 shows the modeled and observed mass balance for the control runs CS2001-1 and EL2001-1.

[64] Overall, the differences between observed and simulated ice thickness are within 16 cm (5.2 cm) in winter (i.e., before the onset of surface melt) at CS (EL). The average error is 0.2 cm (−9.4 cm) after the melt onset (see Table 4 for details). In winter, at both sites, the prescribed snow depth matches the available observations. In summer, at the CS site, the average difference in model and observed snow depth equals 0.2 cm. The simulated and observed snow melt period are consistently short (3 days). On the contrary, at the EL site, the snow cover disappears 7 days too early in the model, leading to an average error in model snow depth equal to −7.6 cm. This problem is further investigated in section 4.4.

[65] The relatively large error in the modeled winter ice thickness at CS2001 may be due either to errors in snow depth or physical properties, for which data are lacking, or in F_w, which was not measured. Snow and oceanic heat supply control the ice growth at the bottom interface. We use a constant value of F_w, while its standard deviation has been shown to be up to 15 W m^{-2} by *Krishfield and Perovich* [2005]. Much larger average error in summer ice thickness is found at EL since the snow disappears too early in the model.

[66] For CS2000-1, since summer 2000 salinity data were contaminated by a flooding event, we only focus on the winter period. The ice thickness model-data agreement is within 2 cm.

4.2. Winter Desalination

[67] Since in winter the salinity profile has a predictable C shape, we compare the model and observed winter salinity profile normalized by ice thickness. We perform the comparison for winter 2000 at CS for which we have the greatest amount of data (10 profiles), for different model configurations (see Figure 8).

[68] The original parameterization of CW88 leads to substantial problems while simulating the winter ice salinity. In agreement with the study of *Cox* [1990], the simulated desalination is much too high, inducing an underestimation of ice salinity of about 2–3‰ in the ice interior. Gravity drainage is too strong in CW88, and we chose to adapt the gravity drainage intensity coefficient δ. Our value, δ_{mod}, is 65% lower than the CW88 value δ_{lab}. This value gave the best balance between a low enough surface salinity and a high enough bottom salinity. If $\delta <$ δ_{mod}, the salinity close to the ice bottom is correct, but it is too high in the upper layers. If δ is higher, the salinity minimum near the ice bottom is substantially too low, as shown by the simulation with the original δ_{lab} value. Reducing δ is of limited utility though. Something is clearly missing from the CW88 model.

[69] No small-scale variability in the vertical salinity profile occurs in the model, while it is often reported in observations.

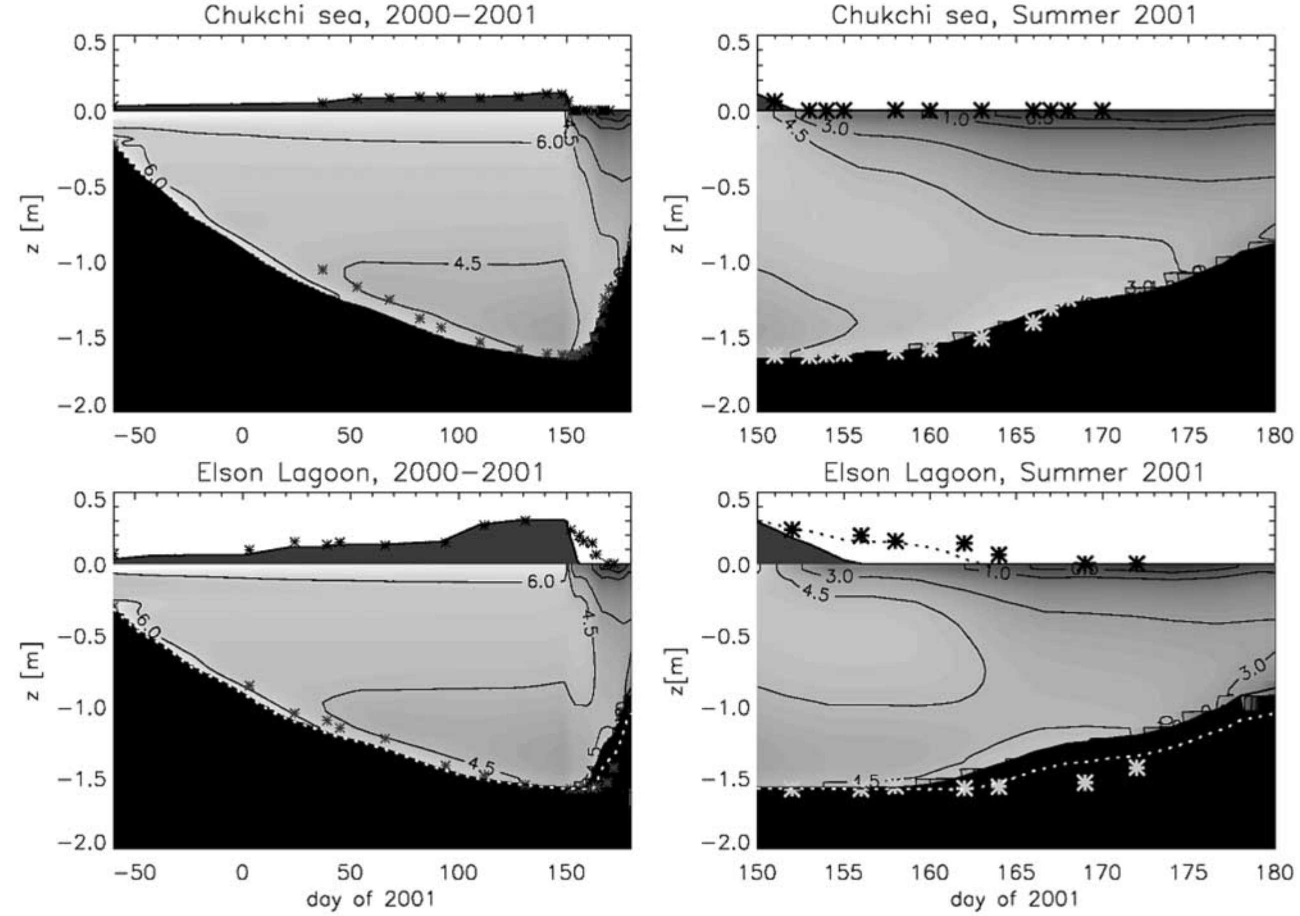

Figure 7. Mass balance and contours of salinity [‰] as simulated by the model at both sites in 2001 (simulations CS2001-1 and EL2001-1). The stars refer to observed values of ice and snow thicknesses. (left) Whole ice growth/melt season. (right) Plots restricted to the summer season. The dotted curves on the Figure 7 (bottom) represent the results of the EL2001-6 simulation (including improved representation of snow physics).

In addition, brine expulsion plays almost no role, a role even smaller than in the study by *Eicken* [1992], since in our model expelled brine is redistributed in the ice. Its main impact is to slightly increase surface salinity by less than 1‰.

4.3. Summer Halothermodynamics

[70] We present the results of the comparison for summer 2001 at both sites. Figure 9 shows the evolution of modeled/observed surface bulk salinity (S_{up}), defined as the salinity in the uppermost 50 cm of the ice. At both sites, the simulated meltwater flushing starts on day 151, simultaneous with surface melt. Then, at the CS site, the flushing continues, while it stops between days 154 and 158 at the EL site were the initial loss of salinity lowers the permeability ($e < e_T$) in the upper layers. Thicker snow at EL contributes to lowering e by delaying warming. The model

Table 4. Differences Between Simulated and Observed Ice Thickness (h_i), Snow Depth (h_s), Bulk Salinity, and Average Temperature of the Uppermost 50 cm of ice (S_{up}, T_{up}) at CS and EL, Summer 2001[a]

		h_i, cm		h_s, cm		S_{up}, ‰		T_{up}, °C		
Run	Description	E	CC	E	CC	E	CC	E	CC	Ice Surface Melt Onset
CS2001-1	Control run	0.2 ± 0.4	0.98	0.2 ± 0.5	0.99	0.01 ± 0.40	0.91	−0.53 ± 0.67	0.94	4 Jun
EL2001-1	Control run	−9.4 ± 11	0.83	−7.6 ± 8.0	0.62	0.57 ± 0.59	0.87	−0.77 ± 0.70	0.93	7 Jun
EL2001-2	Increased snowfall (1)	−5.8 ± 7.4	0.86	−6.3 ± 6.5	0.75	0.69 ± 0.73	0.78	−1.33 ± 0.66	0.86	12 Jun
EL2001-3	Increased k_s and ρ_s (2)	−7.1 ± 9.3	0.85	−6.2 ± 6.8	0.74	0.34 ± 0.80	0.85	−1.11 ± 0.64	0.89	11 Jun
EL2001-4	SW penetration in snow (3)	−4.1 ± 7.2	0.86	−4.5 ± 5.7	0.83	0.85 ± 0.86	0.74	−1.63 ± 0.75	0.81	13 Jun
EL2001-5	Meltwater refreezing (4)	−8.0 ± 10	0.84	−6.8 ± 7.0	0.71	0.04 ± 0.73	0.91	−0.72 ± 0.43	0.96	10 Jun
EL2001-6	(2) + (3) + (4)	−2.7 ± 5.8	0.87	−1.7 ± 3.6	0.94	0.68 ± 0.68	0.80	−1.15 ± 0.43	0.93	14 Jun

[a] The comparison is done for the period between 31 May and 19 June (days 151–170). The date of onset of ice surface melt is also indicated. The experiments EL2001-2 to EL2001-6 are sensitivity experiments to the representation of snow physics in the model (further described in section 4.4.). The average error between model and observations (*E*), the standard deviation of error during the melt period, and the correlation coefficient (CC) are shown.

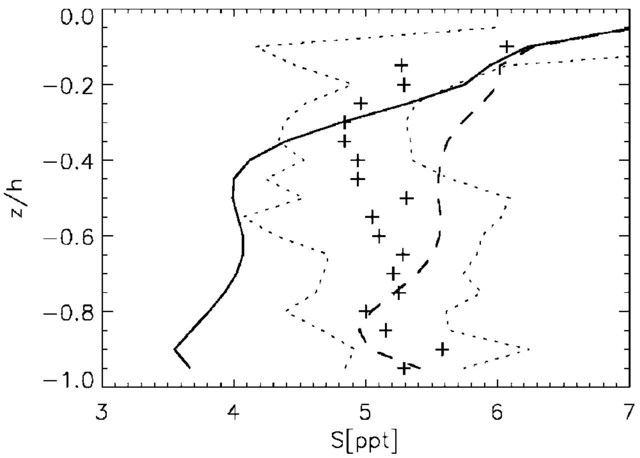

Figure 8. Comparison between model and observed normalized average winter salinity profiles, CS2000. Average over 10 observed profiles, taken between 5 February and 31 May (crosses), and one standard deviation range (dotted lines) are shown. Average simulated profiles (mean taken over the same days) are also presented for different values of δ, which controls the intensity of gravity drainage: *Cox and Weeks* [1988] value δ_{lab} (solid line) and δ_{mod} (dashed line).

surface desalination rate at CS (EL) (i.e., computed in the uppermost 50 cm of ice), is equal to −0.27 (−0.23) ‰ d^{-1}, which is higher than the bulk (i.e., computed over the total thickness of the ice cover) desalination rate, equal to 0.12 (0.08) ‰ d^{-1}. As can be seen in Table 4 the model-data agreement is very good at both sites (error smaller than 1‰ and correlations higher than 0.9). At EL, S_{up} is on average overestimated by 0.57‰, which is of the same order of magnitude as the observation error.

[71] Figures 10 and 11 display the simulated and observed temporal evolutions of the salinity, temperature and brine volume vertical profiles in summer at CS and EL. The overall agreement of the modeled salinity profile with observations is very good. At the CS site, the individual modeled and observed salinities agree within the range of errors, except on day 153. The initial surface salinity decrease is not strong enough in the model. At the EL site, the first modeled profile, typical of the end of winter situation, significantly differs from observations (error of interior salinity is up to 2‰). During the melt period, the shape of the salinity profile is well captured, but, for days 156, 161, 162 and 164, the individual ice salinities are overestimated by up to 1.2‰. On day 169, the observed and simulated salinity profiles agree within the range of observations. The maximal error occurs just after the onset of flushing, which points toward the importance of the early desalination.

[72] The model-data agreement for temperatures corroborates the salinity pattern. At CS, the ice temperature profile is slightly too cold but agrees well with observations (errors less than 0.7°C). Again, the maximal error occurs on day 153, with significant underestimation of the temperature by the model (by up to 3°C). Similarly, at the EL site, the ice temperatures are underestimated by the model at the beginning of the melt period, and then agree with observations within 0.5°C.

[73] The agreement between observed and model brine volume vertical profiles is not as good as what we had for salinity and temperature. Differentiating (4), we get

$$\Delta e = -\frac{\mu}{T}\Delta S + \mu \frac{S}{T^2}\Delta T, \qquad (11)$$

where T is a temperature in °C. Equation (11) indicates that the error in brine volume is dominated by temperatures close to the seawater freezing point. The overall underestimation in brine volume at both sites indicate that ΔT dominates the error in brine volume at both sites. Nevertheless, the model captures well the time when the ice first reaches the permeability threshold ($e > e_T$).

[74] In summary, when the snow cover is thin and disappears quickly (CS2001), the model manages to simulate the ice mass balance, salinity and temperature profiles. If the snow cover is thick and melts slowly, then the model fails to reproduce the snow and ice mass balance but still does a reasonable job in simulating the salinity and temperature profiles. The upper ice layers temperatures are consistently underestimated at the onset of the melt period.

4.4. Sensitivity of Summer Halothermodynamics to the Representation of the Snow in the Model

[75] In this section, we study the sensitivity of the simulation to snow physics at EL in summer 2001. We investigate whether it is possible to improve the model

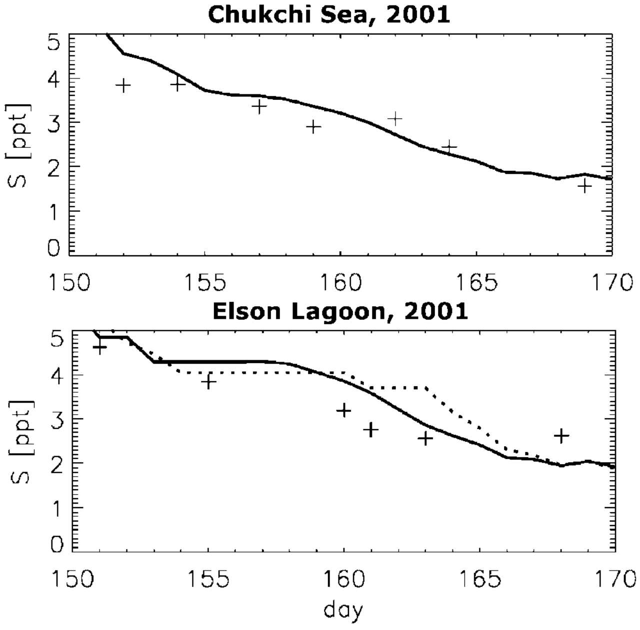

Figure 9. Observed (crosses) and simulated (lines) surface bulk salinities S_{up} (i.e., restricted to the upper 50 cm of ice) in summer 2001 at (top) CS (simulation CS2001-1) and (bottom) EL. On Figure 9 (bottom), the results of simulations EL2001-1 (solid line) and EL2001-6 (dashed line) are shown.

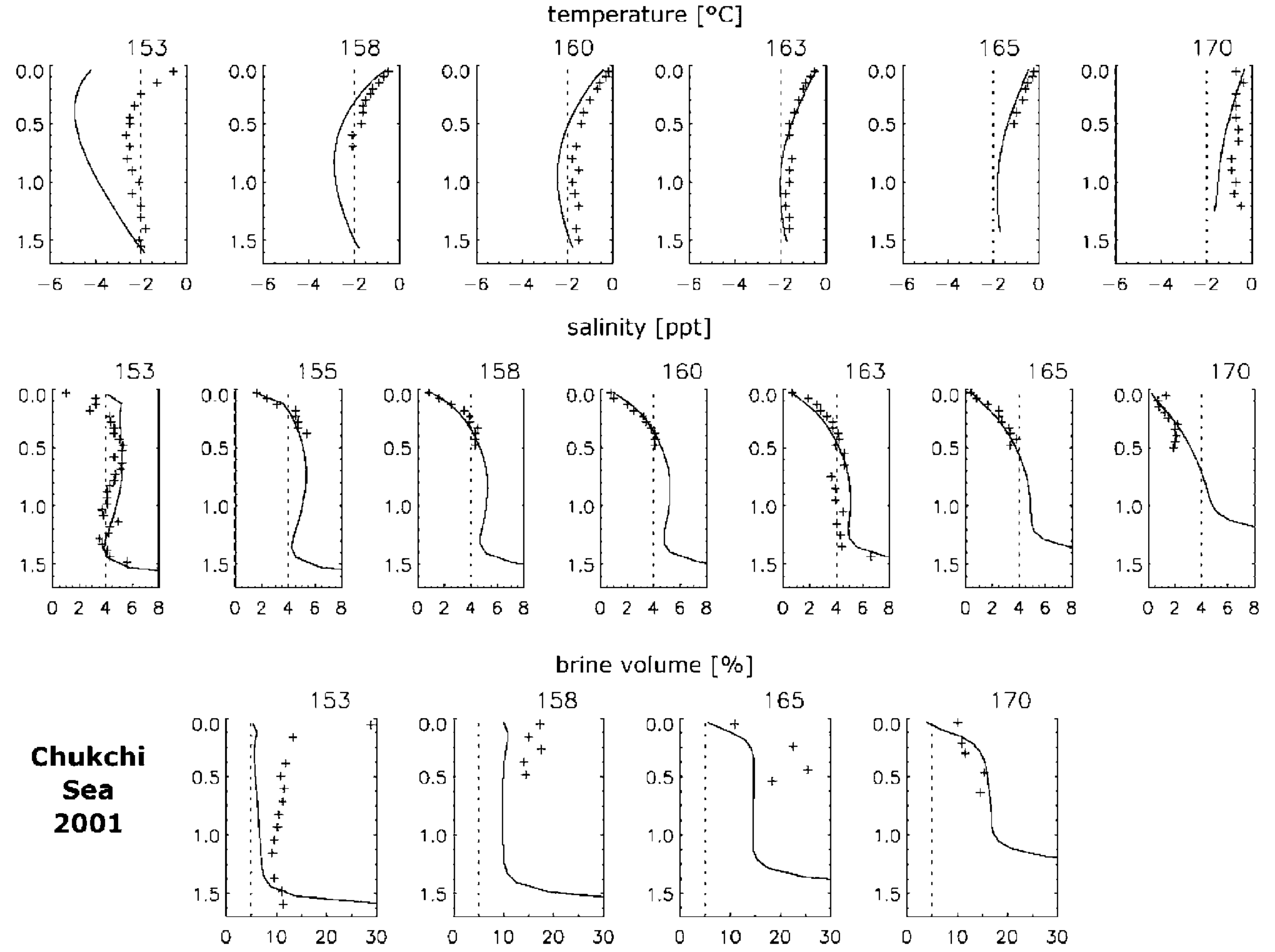

Figure 10. Observed (stars) and simulated (lines) vertical temperature [°C], salinity [‰], and brine volume [%] profiles at CS during the early melt period of 2001 (simulation CS2001-1). Vertical axis refers to depth in the ice [m]. The numbers at the top of the individual plots indicate the number of the day in the year. Brine volume is computed from equation (4).

summer snow mass balance while maintaining or improving the desalination process. We perform five sensitivity experiments (EL2001-2, -3, -4, -5, -6) presented in Table 4.

[76] In EL2001-2, an extra 2 cm d^{-1} of snowfall is added for days 155–165, and the results change very little. The absolute value of the average error in snow depth is only reduced by 1.3 cm (from 7.6 cm). Therefore the omission of solid precipitation during the melt period is unlikely to be responsible for the model-data discrepancy.

[77] For EL2001-3, several studies [e.g., *Sturm et al.*, 2002; *Huwald et al.*, 2005b] indicate that the deepest snow layers tend to be denser and therefore more conductive, due to snow compaction and refreezing. These layers persist in summer after a few days of melt. In EL2001-3, we use ρ_s = 400 kg m^{-3} and k_s = 0.40 W m^{-1} K^{-1} to take this effect into account. In order to maintain the same bottom ice growth as in the control run, we only modify the snow thermal conductivity and density when snow melts.

[78] In EL2001-4, snow transmits radiation, as suggested by *Grenfell and Maykut* [1977]. In EL2001-4, we solve Beer's law in the snow. As Grenfell and Maykut suggest, we use i_o = 0.15 and use an extinction coefficient κ_s = 15 m^{-1} in the snow.

[79] In EL2001-5, meltwater percolates and refreezes, leading to superimposed ice formation. Superimposed ice formation is much more likely when the snow layer is thick (H. Eicken, personal communication). Superimposed ice was present at the EL site, at the snow-ice interface from 5 to 11 June (days 156–161), but it was not observed at CS at the same period. In our model, when the snow melts, the resulting meltwater is immediately sent to the ocean, instead of being trapped in the snow or at the ice surface. We thus lose meltwater, which might otherwise refreeze in the snow or at the ice surface and form superimposed ice. Consequently, it may increase the snow density and the required energy to melt the snow. In addition, refreezing meltwater increases heat transport to the ice. In the EL2001-5 simulation, when snow starts to melt, we assume half of the meltwater refreezes at the ice surface, as suggested by superimposed ice fractions derived from $\delta^{18}0$ values in the

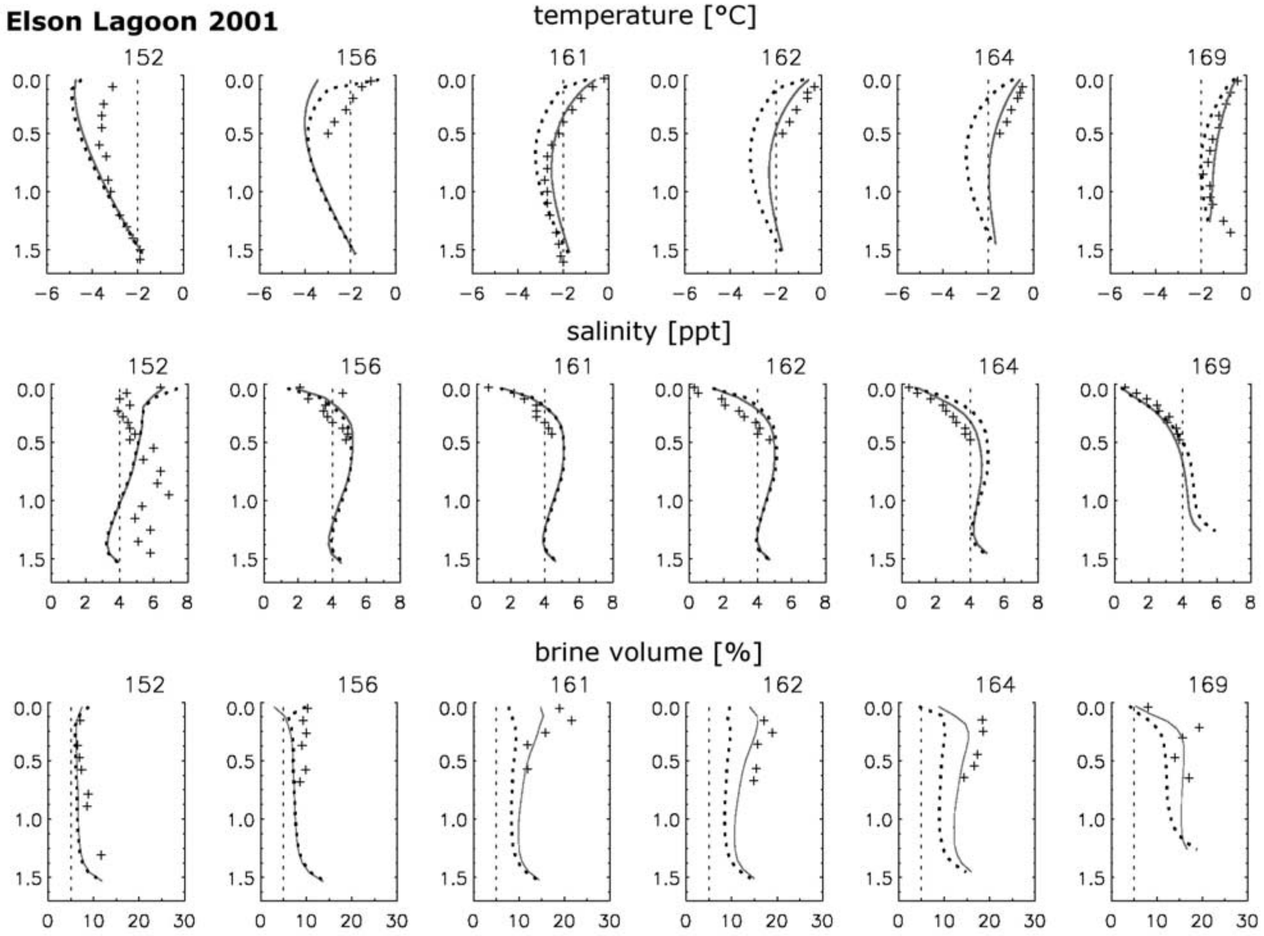

Figure 11. Same as Figure 10, but at EL. EL2001-1 (gray solid curves) and EL2001-6 simulations (black dashed curves) are shown.

uppermost ice layers by *Eicken et al.* [2004] and direct observations of *Nicolaus et al.* [2003]. Effectively the rate of snow loss is reduced and instead the uppermost ice layers are warmed by an equivalent amount of heat. This amount of energy per unit of area Q_{rf}, representing the thermal role of refreezing on the snow-ice interface heat balance, is given by

$$Q_{rf} = 0.5\rho_s L_0 \Delta h_s^{<0}; \qquad (12)$$

$L_0 = 334$ kJ kg^{-1} is the massive latent heat of pure ice. $\Delta h_s^{<0}$ is the daily decrease in snowmelt.

[80] In the EL2001-6 simulation, we combine the three additional snow physical features used in the simulations EL2001-3, -4, and -5. Taken separately, the extra snow features reduce snowmelt, maintain the snow cover during a longer period, reducing errors. Improving the snow depth simulation consistently results in better ice thickness, since ice does not melt instead of snow. Including the penetration of radiation through the snow (EL2001-3) induces the most remarkable reduction in the error in snow depth (3.1 cm). The effects of combined extra snow features add up (EL2001-6) and lead to an overall reduction in snow depth error by 5.9 cm, leading to a much smaller average error (1.7 cm). In Figure 7, the temporal evolution of snow depth in EL2001-6 can be compared to EL2001-1.

[81] The impact of the extra snow features on temperature and salinity profiles is not always positive. Compared to the control run, in EL2001-3 and EL2001-4, the model temperature profile is deteriorated. The heat supply to the upper ice layers increases, due to larger heat conduction (transmitted radiation) in EL2001-3 (EL2001-4). In these two simulations though, the increased heat supply is smaller than the reduced supply of sensible heat due to the deeper insulating snow cover. This implies colder temperature in the uppermost ice layers. Increasing the snow thermal conductivity and density (EL2001-3) does not lead to any remarkable change in the simulation of the ice desalination. Adding the penetration of radiation through the snow (EL2001-4) significantly increases the error in ice salinity. The significantly deeper snow cover in EL2001-4 induces much colder temperatures, lower brine volume and fewer desalination.

Table 5. Description of the Sensitivity Experiments to Internal Parameters i_0, ϕ, and e_T

Run	i_0	ϕ	e_T
CS2001-1	0.30	0.30	5%
CS2001-2	0.00	0.30	5%
CS2001-3	0.50	0.30	5%
CS2001-4	0.30	0.20	5%
CS2001-5	0.30	0.50	5%
CS2001-6	0.30	0.30	8%
CS2001-7	0.30	0.30	10%

[82] In EL2001-5, superimposed ice formation slightly warms the temperature of the upper ice layers. Though the ice is still too cold in EL2001-5, the simulation of the salinity profile is much better than in the control run. The warmer uppermost ice layer is more permeable and therefore more prone to desalination.

[83] The combined snow features (EL2001-6) only slightly deteriorate the temperature and salinity profile, as can be seen in Figure 11. The overall quality of the simulation of the salinity and temperature profile is conserved. While penetration of radiation seems to play a key role in maintaining deeper snow, the thermal effect of meltwater refreezing is of primary importance for temperature and salinity. It provides an efficient means to transfer heat to the uppermost ice regions and to maintain warm and permeable ice at the surface. Other source of errors, like the uncertainty in SW radiation due to errors in cloud cover, may also affect the upper ice layers temperatures, desalination and melt.

4.5. Sensitivity of Summer Desalination to Meltwater Flushing Parameters (i_0, ϕ, e_T)

[84] In order to get a better physical understanding of the summer sea ice desalination, we assess in this section the model sensitivity to the parameters i_0, ϕ and e_T. Details about the experiments (run in the CS2001 conditions) are shown in Table 5. Results are shown in Figure 12.

[85] According to equation (10), the desalination rate by flushing depends on Q, on $e(z)$ and on $d\sigma/dz$. Depending on the minimum brine volume e_{min}, flushing occurs or not. Q is the same throughout all ice layers and is proportional to ϕ and the surface melt rate. For a given Q, ice layers with larger brine volume desalinate more slowly. $d\sigma/dz$ is conditioned by the temperature profile, according to equation (2). Depending on the shape of the temperature profile, $d\sigma/dz$ can be positive or negative, which in turn modulates the sign of dS/dt.

[86] Solar radiation penetrating inside the ice warms the inner ice layers, instead of contributing to the surface energy budget and surface melt. A higher i_0 therefore induces less surface melt, smaller Q but warmer upper ice layers.

[87] In the CS2001-2 simulation (i_0 = 0), the surface melt and desalination are initially very intense (see Figure 12, a1). After 5 days of melt, the uppermost ice layers have a relatively low salinity and are relatively cold, such that $e < e_T$ (see Figure 12, a2). In other words, an impervious cold surface layer has formed. The desalination is then discontinuous, alternating between the melt and the formation of a new surface impervious layer. After 20 days into the melt period, the salinity is very low at the surface, but remains high in the bottom layers. First, the shape of the brine volume profile (see Figure 12, a5), with low brine volumes at the surface and high brine volumes at the ice bottom, implies that the desalination effect is the strongest close to the ice surface. Second, the absence of penetrating radiation allows the C-shaped temperature profile to persist longer (see Figure 12, a3). The brine salinity gradient therefore remains negative (positive) in the upper (lower) ice layers (see Figure 12, a4). Therefore the brine salinity always decreases (increases) in the uppermost (bottommost) ice layers. Note that this kind of impervious layer also forms in the EL2001-1 simulation but only during days 154–158 and might be an incentive to the accumulation of meltwater at the surface and the formation of superimposed ice.

[88] In the CS2001-3 simulation (i_0 = 0.5) simulation, surface melt and Q are smaller. Therefore the desalination is less intense and lasts longer. Higher salinity and brine volume can be found close to the surface. There is a period of 10 days during which the temperature profile is C-shaped. Therefore the brine salinity gradient is negative (positive) in the uppermost (bottommost) layers. This period has a similar length in CS2001-1 and CS2001-3. Since Q is smaller in CS2001-3, in the uppermost (bottommost) layers the brine salinity will be higher (lower) than in CS2001-1.

[89] A smaller ϕ reduces Q. Therefore the simulation CS2001-4 (ϕ = 0.20) has qualitatively the features of the CS2001-3 simulation described in the previous paragraph. A larger ϕ induces a larger Q and stronger and quicker desalination. This results in smaller (larger) ice salinity in the uppermost (bottommost) ice layers. Compared to the CS2001-2 (i_0 = 0) simulation described earlier, owing to the penetration of solar radiation, the inner ice layers remain warm enough and no surface impervious layer is formed.

[90] The permeability threshold e_T affects mainly the time of the onset of flushing (see Figure 12c). With $e_T \leq 5\%$, flushing starts when surface melt starts. If e_T = 8% (10%), the flushing starts 5 (10) days after surface melt.

5. Summer Meltwater Budget

[91] According to our model, during the first 21 days of the melt period (days 151–171), surface meltwater percolates through bare ice at the rate of 0.36–0.56 cm d^{-1} or 76–117 L m^{-2} (see Table 6). In other words, on bare ice, on average 26.4% of the surface meltwater (produced on bare ice) must flush through the ice to simulate the observed salinity profiles during the first 21 days of the melt period. The remainder of the meltwater is either discharged into the mixed layer through cracks and leads, percolates through ponded ice, or accumulates in surface and underwater melt ponds by lateral drainage. By comparison, from observations, *Eicken et al.* [2002] deduce that over the summer 12% of the total meteoric water is retained by bare ice. This tends to corroborate that much of the vertical percolation occurs during the early stage of melt.

6. Discussion and Conclusions

6.1. Observations of Early Summer Desalination

[92] We examined two years (2000 and 2001) of early summer sequences of salinity profile measured from landfast ice cores at two sites in Point Barrow, Alaska. We see a quick desalination, starting at the onset of melt. This desalination for bare ice causes a transition between the

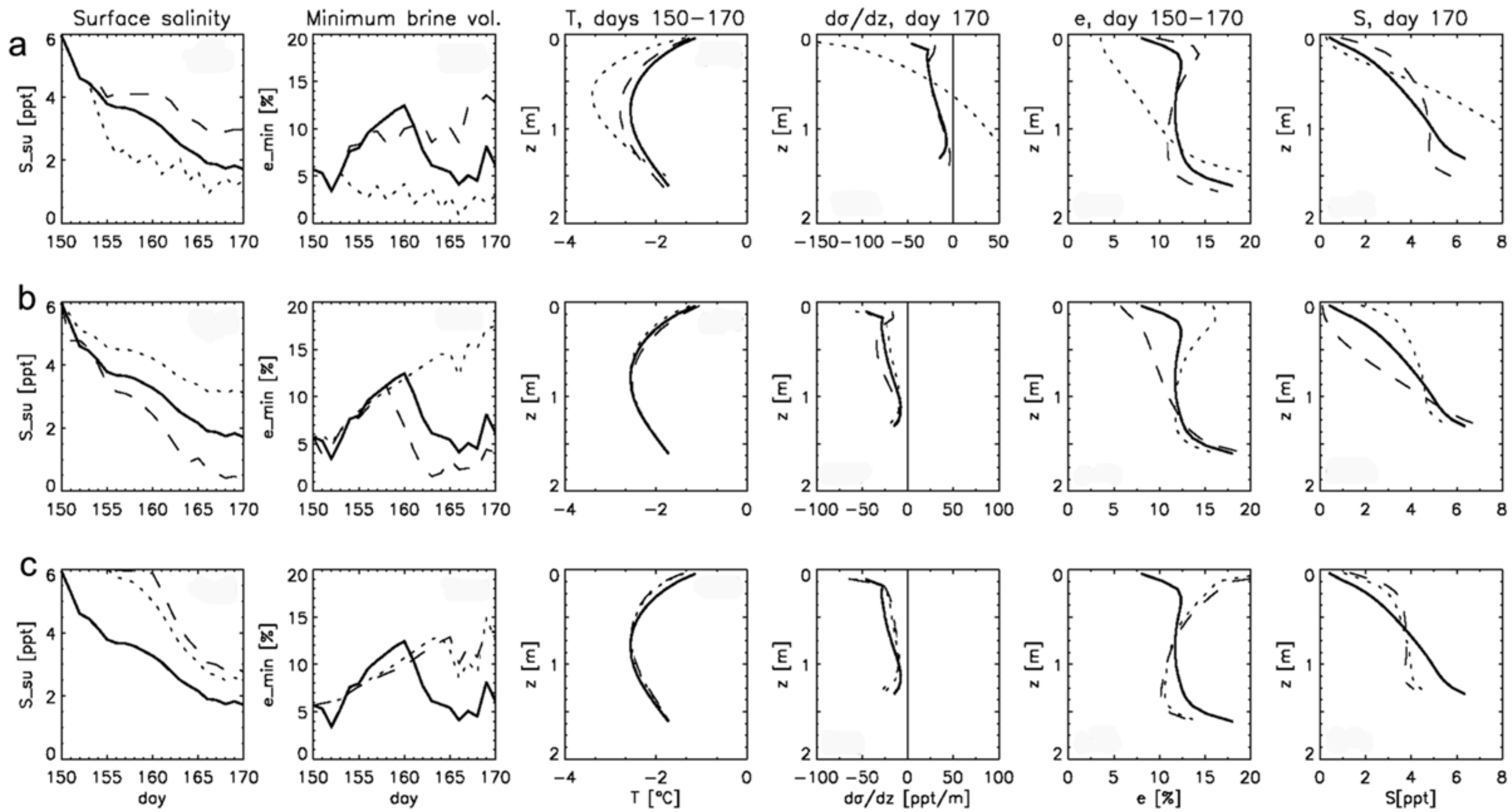

Figure 12. Sensitivity experiments (a) to i_0: CS2001-2 (dotted line); CS2001-1 (solid line); CS2001-3 (dashed line). (b) Sensitivity to ϕ: CS2001-4 (dotted line); CS2001-1 (solid line); CS2001-5 (dashed line). (c) Sensitivity to e_T: CS2001-1 (solid line); CS2001-6 (dotted line); CS2001-7 (dashed line). For each sensitivity experiment, the temporal evolution of surface salinity (i.e., bulk salinity of the uppermost 50 cm of ice) and of minimum brine volume is shown. The vertical profiles of temperature (averaged over days 150–170), of $\partial\sigma/\partial z$ (day 170), of brine volume (averaged over days 150–170) and of salinity (day 170) are also plotted.

Table 6. Simulated Total Mass of Surface Meltwater Percolating Through the Ice (Total Flow and Specific Contributions From Snow and Ice) in Early Summer 2001 (1–20 June) and Daily Average Percolating Flux[a]

	Snow/Ice, kg m^{-2}	Snow, kg m^{-2}	Ice, kg m^{-2}	Average Percolating Flux
Chukchi Sea	116.9	10.8	106.1	5.56 kg $m^{-2}d^{-1}$
	28.8%	27%	29.1%	0.56 cm d^{-1}
Elson Lagoon	76.4	17.8	58.0	3.63 kg $m^{-2}d^{-1}$
	24.0%	17.8%	27.6%	0.36 cm d^{-1}

[a] The percentages represent the ratio of total (respectively snow, ice) percolating meltwater flow to the total (respectively snow/ice) meltwater mass formed at the surface. Simulations CS2001-1 and EL2001-4 are used.

C-shaped FY ice salinity profile and the typical MY salinity profile, characterized by the upper 50 cm of almost fresh ice. After 12 days (averaged over the CS2000, CS2001, and EL2001 desalination sequences), the bulk salinity of the upper 50 cm of ice first drops under 3‰ and the typical MY ice profile forms, then remains nearly unchanged through the end of the investigated period (first 21 days of melt). A longer desalination sequence of melting FY ice described by *Eicken et al.* [2002] shows a further desalination, leading to practically fresh ice after 20 more days of melt. This further desalination is prompted by convective overturning of freshwater coming from the ice bottom into the brine network.

[93] In ponded ice, the salinity profile tends to a vertically constant profile with S = 2‰. This points to a different halothermodynamic regime, which is beyond the scope of the present study.

[94] The observed desalination signal is significantly larger than observation errors. In addition to systematic extraction errors (about 10–20% of the initial salinity in summer), the fact that subsequent ice cores were taken from different places was certainly not ideal. During early summer, horizontal variability in salinity at a particular depth (0.34‰) was found to be 2–3 times smaller than in winter. We attribute it to the fact that the ice desalination occurs everywhere and therefore homogenizes the profiles. We suspect summer horizontal variability in ice salinity is larger than what was directly observed. In particular, snow cover variability can induce variability in superimposed ice formation, which affects the amount of percolating water. In addition, other kinds of flooding events may scramble the pattern. New instruments able to measure the sea ice salinity, as for example, based on impedance measurements [see, e.g., *Notz et al.*, 2005], should be very useful at monitoring the horizontal variability of sea ice salinity.

6.2. Modeling the Winter Sea Ice Salinity Profile

[95] Our prognostic salinity model for Arctic undeformed bare ice, based on the model of CW88. The simulation of winter salinity profiles reveals that the original CW88 model has some deficiencies, as already mentioned by *Cox* [1990]. As it is proposed, CW88 leads to correct desalination in the first two weeks of ice growth. After that, the gravity drainage is too intense and leads to excessively small salinity close to the ice-ocean interface. The δ factor, describing the impact of the unstable temperature gradient on the ice desalination, had to be reduced by 65% to give better bottom salinity. The fact that the CW88 parameterization of gravity drainage is valid only for early stages of ice growth is not surprising. The data on which this parameterization was based [*Cox and Weeks*, 1975] were taken from laboratory ice, only up to 20 days old, and probably are not representative of the overall winter period. The corrected δ value suggested by our study is more representative of the average winter behavior, but not of the initial desalination, which is too weak.

[96] In CW88, gravity drainage is empirical. A feature absent in our simulations is the double C shape that we see in the observations (see Figure 3a). *Notz* [2005] gives an explanation of this feature, based on the concept of a permeability-associated mush-Rayleigh number that cycles through subcritical and supercritical regimes, but this is much more sophisticated than warranted by the parameterizations used in our model.

[97] The present data show that in the ice interior, the salinity is practically constant with a value of about 5‰, which suggests that the winter desalination mechanisms stop when this value is reached. *Cox* [1990], suggested to add seawater suction (the reverse process of brine expulsion) to the CW88 model. When the ice is warmed, brine would be sucked up from the underlying seawater, which has never been observed. Furthermore, this mechanism is not well motivated and not supported by observations. Still, the question of the mechanism beyond gravity drainage (brine convection, diffusion, capillarity effects in brine tubes) leading to a stable C-shaped profile is not elucidated. Further field and model studies are required to answer this question. *Mercier et al.* [2005] show that diffusion might dominate in certain years in the Southern Ocean. A more physical modeling approach, based on mushy layer theory, should also help to answer this question [see, e.g., *Oertling and Watts*, 2004; *Notz*, 2005].

6.3. Modeling the Summer Arctic Bare Ice Mass Balance and Salinity Profile

[98] The external forcing (LW radiation, and oceanic heat flux) was tuned to provide a reliable simulation of the sea ice mass balance. In summer, when the snow cover is thin (at the CS site), the model and observed ice thickness and snow depth are in close agreement (average error smaller than 0.5 cm). When snow is deep (at the EL site), the snow melts 10 days too early and the ice is on average 9.4 cm too thin. In both cases, the salinity profile is well captured by the model, but the upper ice interior is slightly too cold during the first 10 days of the melt period. Even though the model captures the brine volume vertical profile relatively well, the relative errors in brine volume are higher than in salinity and temperature because the error in brine volume, depending on $1/T^2$, are maximal close to the freezing point. Direct observations of brine volume would help to further investigate this problem.

[99] Our model includes an original parameterization of summer flushing. Flushing is defined as the vertical component of the translation/diffusion movement of the brine salinity structure in the brine network, triggered by an interconnected brine network and the availability of freshwater at the surface. Because the hydraulic flow depends mostly on ice permeability rather than meltwater produc-

tion, we suggest that flushing can be considered instantaneous compared to one-day time step.

[100] The simulated summer bare ice desalination is in agreement with observations, when the fraction ϕ of available meltwater percolating into the brine network was set to 30%. This tuning parameter partitions the available meltwater between lateral and vertical percolation. Its value is probably dependent on the time step. We imagine, for example, that if the diurnal cycle is resolved, the ice could be permeable at noon and impervious at night. The value used here represents the daily average amount of meltwater used in vertical desalination.

[101] A significant part of errors in the model mass balance, temperature and salinity at EL is also due to the errors in the forcing (in particular the ocean heat flux). On the other hand, the rough representation of the snow cover in the model is also of primary importance. The sensitivity experiments in section 4.4 suggest that a better representation of snow physics and of the fate of surface meltwater in the model would improve not only the simulation of the snow cover but also the simulation of ice mass, heat and salt balance. Penetration of radiation through the snow, snow compaction and subsequent increase in snow thermal conductivity, as well as superimposed ice formation, slow the melt of snow and increase the heat transfer to the ice interior. Penetrating radiation has the largest impact on snow depth. Refreezing of surface meltwater is important to maintain the uppermost ice warm under a thick, insulating snow cover. The simulations show at EL that a sufficient amount of heat transferred through the snow is compulsory to open the brine network in the upper ice layers.

6.4. Flushing and Superimposed Ice Formation

[102] In our simulations the first flushing event occurs at the same time as the onset of surface melt. At the CS site, the brine network is always open and flushing is continuous. At the EL site, helped by the initial decrease in S and insulated from the surface by a thick snow cover, the upper brine network closes for a few days, leaving no way to meltwater and favoring superimposed ice formation. These differences suggest a series of desalination regimes that depend on snow depth as follows:

[103] 1. A very thick snow cover is present, and there is no surface melt. No percolation of meltwater occurs, the profile remains C-shaped. Such profiles were among second-year ice profiles observed in the Weddell Sea by *Eicken* [1998].

[104] 2. A thick snow cover is present, melting at the surface. The upper ice layers are efficiently insulated and thus cold enough at the snowmelt onset so that they are impervious to the incoming meltwater percolating through the snow. In contact to the impervious, relatively cold surface, the percolating meltwater has the potential to form a fresh layer of superimposed ice. This leads to a profile with a “7” shape (i.e., fresh at the surface and with more or less constant salinity inside the ice). Profiles from the Weddell Sea taken in summer by *Haas et al.* [2001] correspond to this description. This is a reason why more superimposed ice is found under thick snow layers [see, e. g., *Eicken et al.*, 2004]. The thick superimposed ice layers observed in the Baltic Sea [see, e.g., *Granskog et al.*, 2006] may also be explained because the ice is almost fresh there and therefore impervious to meltwater percolation.

[105] 3. A thick snow cover is present, melting at the surface, but the upper sea ice layers are permeable at the melt onset. Initially, meltwater percolates and creates a profile with a more or less linear shape at the surface. Since the upper ice layers are well insulated from the surface by the thick snow cover, they are relatively cold and the desalination may render the upper ice layers impervious. Superimposed ice formation may then start for a few days, until the ice layers are warm enough again to be permeable. This is the situation found at CS2000 and EL2001.

[106] 4. A thin snow cover is present, melting at the surface. The upper sea ice layers are permeable at the melt onset. Flushing is continuous in these situations. Meltwater percolates but does not form superimposed ice. This is the situation found at CS2001.

6.5. Meltwater Balance

[107] The modeled desalination is compatible with meltwater storage in the ice data of *Eicken et al.* [2002]. Our model suggests that 24.5% of the basin-scale meltwater is stored in bare ice in the early stages of summer (20 days), while Eicken et al found a value for the whole summer of 12%. The discrepancy between the two values might signify that the vertical seepage of meltwater in the ice decreases after the early stage of melt because bare ice becomes much more permeable as it desalinates. Another explanation is that some of the bare ice melts and releases its meltwater content to the mixed layer. Thus the freshwater flow coming from the bare ice surface melt is excessive to desalinate the ice.

6.6. Perspectives

[108] The present study underlines that further field campaigns with a large focus, joining several aspects of the ice cover physics (e.g., snow and ice mass balance, freshwater pathways, ice temperature, salinity and brine volume) are a powerful tool to constrain thermodynamic sea ice models.

[109] In a parallel study [*Vancoppenolle et al.*, 2006], we show that the halothermodynamic model presented here is able to simulate MY ice salinity profile and reaches a quasi-equilibrium after 10 years of simulation (i.e., the present model does not drift). Therefore it should be able to simulate the features of the Arctic bare ice salinity profile in climate models, where particular care should be taken to ensure heat and salt conservation.

[110] Nevertheless, the present model is only a step toward a better representation of the thermodynamics of the polar snow-ice cover. Future model development should focus on the physics of the snow cover, the meltwater pathways and storage and the gravity drainage of brine. Another extension of the model could be to include a melt pond scheme, such as from *Taylor and Feltham* [2004].

[111] **Acknowledgments.** The authors would like to thank Hajo Eicken for providing the data and helpful comments on various aspects of this work; Bruno Tremblay, Dirk Notz, Jean-Louis Tison, Valérie Dulière, and Hugues Goosse for discussions which significantly helped to improve the quality of the present manuscript; the National Oceanic and Atmospheric Administration’s (NOAA) Climate Monitoring and Diagnostics Laboratory (CMDL) for providing the meteorological data.

M. Vancoppenolle is Research Assistant at the Belgian National Fund for Industrial and Agricultural Research and is supported by the Belgian Federal Science Policy Office. This study was carried out within the scope of the project A Second-Generation Model of the Ocean System, funded by the Communauté Française de Belgique (Actions de Recherche Concertées, contract ARC 04/09-316), and the project Climate Change and Cryosphere, which is supported by the Ministère Français de la Recherche (Action Concertée Incitative Changement Climatique). C.M.B. gratefully acknowledge the support of the National Science Foundation through grants ATM0304662 and OPP0454843.

References

Aagaard, K., and E. C. Carmack (1989), The role of sea ice and other fresh water in the Arctic circulation, *J. Geophys. Res.*, *94*, 14,485–14,498.

Ackley, S. F., and C. W. Sullivan (1994), Physical controls on the development and characteristics of Antarctic sea ice biological communities—A review and synthesis, *Deep Sea Res.*, *41*, 1583–1604.

Andreas, E. L., and S. F. Ackley (1981), On the differences in ablation seasons of the Arctic and Antarctic sea ice, *J. Atmos. Sci*, *39*, 440–447.

Assur, A. (1958), Composition of sea ice and its tensile strength, in *Arctic Sea Ice*, *Publ. Natl. Acad. Sci. U.S.A.*, *598*, 106–138.

Berliand, M. E., and T. G. Berliand (1952), Determining the net long-wave radiation of the Earth with consideration of the effect of cloudiness (in Russian), *Isv. Akad. Nauk SSSR, Ser. Geofiz.*, *1*, 64–78.

Berliand, M. E., and T. G. Strokina (1980), *Global Distribution of the Total Amount of Clouds* (in Russian), 71 pp., Hydrometeorol. Publ., St. Petersburg, Russia.

Bitz, C. M., and W. H. Lipscomb (1999), An energy-conserving thermodynamic model of sea ice, *J. Geophys. Res.*, *104*, 15,669–15,677.

Cottier, F., H. Eicken, and P. Wadhams (1999), Linkages between salinity and brine channel distribution in young sea ice, *J. Geophys. Res.*, *104*, 15,859–15,871.

Cox, G. F. N. (1990), Verification results of the Cox and Weeks sea ice salinity prediction model (abstract), in *Sea Ice Properties and Processes*, *CRREL Monogr.*, vol.90–1, edited by S. F. Ackley and W. F. Weeks, U.S. Army Cold Reg. Res. and Eng. Lab., Hanover, N. H.

Cox, G. F. N., and W. F. Weeks (1974), Salinity variations in sea ice, *J. Glaciol.*, *13*, 109–120.

Cox, G. F. N., and W. F. Weeks (1975), Brine drainage and initial salt entrapment in sodium chloride ice, *CRREL Rep. 345*, 85 pp., U. S. Army Cold Reg. Res. and Eng. Lab., Hanover, N. H.

Cox, G. F. N., and W. F. Weeks (1986), Changes in the salinity and porosity of sea ice samples during shipping and storage, *J. Glaciol.*, *32*, 371–375.

Cox, G. F.N., and W. F. Weeks (1988), Numerical simulation of the profile properties of undeformed first-year sea ice during the growth season, *J. Geophys. Res.*, *93*, 12,449–12,460.

Eicken, H. (1992), Salinity profiles of Antarctic sea ice: Field data and model results, *J. Geophys. Res.*, *97*, 15,545–15,557.

Eicken, H. (1998), Factors determining microstructure, salinity and stable-isotope composition of Antarctic sea ice: Deriving modes and rates of ice growth in the Weddell Sea, in *Antarctic Sea Ice: Physical Processes, Interactions and Variability*, *Antarct. Res. Ser.*, vol. 74, edited by M. O. Jeffries, pp. 89–122, AGU, Washington, D. C.

Eicken, H. (2003), From the microscopic to the macroscopic to the regional scale: Growth, microstructure and properties of sea ice, in *Sea Ice—An Introduction to Its Physics, Chemistry, Biology and Geology*, edited by D. N. Thomas and G. S. Dieckmann, pp. 22–81, Blackwell, Malden, Mass.

Eicken, H., M. A. Lange, and G. S. Dieckmann (1991), Spatial variability of sea ice properties in the northwestern Weddell Sea, *J. Geophys. Res.*, *96*, 10,603–10,615.

Eicken, H., M. Lensu, M. Leppäranta, W. B. Tucker III, A. J. Gow, and O. Salmela (1995), Thickness, structure and properties of level summer multiyear ice in the Eurasian sector of the Arctic Ocean, *J. Geophys. Res.*, *100*, 22,697–22,710.

Eicken, H., H. R. Krouse, D. Kadko, and D. K. Perovich (2002), Tracer studies of pathways and rates of meltwater transport through Arctic summer sea ice, *J. Geophys. Res.*, *107*(C10), 8046, doi:10.1029/2000JC000583.

Eicken, H., T. C. Grenfell, D. K. Perovich, J. A. Richter-Menge, and K. Frey (2004), Hydraulic controls of summer Arctic pack ice albedo, *J. Geophys. Res.*, *109*, C08007, doi:10.1029/2003JC001989.

Frankenstein, G., and R. Garner (1967), Equations for determining the brine volume of sea ice from −0.5°C to −22.9°C, *J. Glaciol.*, *6*, 943–944.

Frey, K., H. Eicken, D. K. Perovich, T. C. Grenfell, B. Light, L. H. Shapiro, and A. P. Stierle (2001), Heat budget and decay of clean and sediment-laden sea ice off the northern coast of Alaska, paper presented at Port and Ocean Engineering in the Arctic Conference (POAC'1) Ottawa, Ont., Canada.

Gerland, S., J. G. Winther, J. B. Ørbaeck, and B. V. Ivanov (1999), Physical properties, spectral reflectance and thickness development of first year fast ice in Kongsforden, Svalbard, *Pol. Res.*, *18*, 275–282.

Golden, K. M., S. F. Ackley, and V. I. Lytle (1998), The percolation phase transition in sea ice, *Science*, *282*, 2238–2241.

Goosse, H. (1997), Modeling the large-scale behavior of the coupled ocean-sea ice system, Ph.D. thesis, 231 pp., Univ. Catholique de Louvain, Louvain-la-Neuve, Belgium.

Gow, A. J., S. F. Ackley, W. F. Weeks, and J. W. Govoni (1982), Physical and structural characteristics of Antarctic Sea ice, *Ann. Glaciol.*, *3*, 113–117.

Gow, A. J., S. F. Ackley, K. R. Buck, and K. M. Golden (1987), Physical and structural characteristics of Weddell Sea pack ice, *CRREL Rep. 87-14*, 71 pp., U.S. Army Cold Reg. Res. and Eng. Lab., Hanover, N. H.

Granskog, M. A., T. Vihma, R. Pirazzini, and B. Cheng (2006), Superimposed ice formation and surface energy fluxes on sea ice during the spring melt-freeze period in the Baltic Sea, *J. Glaciol.*, *52*, 119–127.

Grenfell, T. C., and G. A. Maykut (1977), The optical properties of ice and snow in the Arctic basin, *J. Glaciol.*, *18*, 445–463.

Haas, C., D. N. Thomas, and J. Bareiss (2001), Surface properties and processes of perennial Antarctic sea ice in summer, *J. Glaciol.*, *47*, 613–625.

Huwald, H., L.-B. Tremblay, and H. Blatter (2005a), A multilayer sigma-coordinate thermodynamic sea ice model: Validation against Surface Heat Budget of the Arctic Ocean (SHEBA)/Sea Ice Model Intercomparison Project Part 2 (SIMIP2) data, *J. Geophys. Res.*, *110*, C05010, doi:10.1029/2004JC002328.

Huwald, H., L.-B. Tremblay, and H. Blatter (2005b), Reconciling different observational data sets from Surface Heat Budget of the Arctic Ocean (SHEBA) for model validation purposes, *J. Geophys. Res.*, *110*, C05009, doi:10.1029/2003JC002221.

Kovacs, A. (1996), Sea ice, part I, Bulk salinity versus ice floe thickness, *CRREL Rep. 96-7*, 16 pp., U.S. Army Cold Reg. Res. and Eng. Lab., Hanover, N. H.

Kovacs, A. (1997), Estimating the full-scale flexural and compressive strength of first-year sea ice, *J. Geophys. Res.*, *102*, 8681–8689.

Krishfield, R. A., and D. K. Perovich (2005), Spatial and temporal variability of oceanic heat flux to the Arctic ice pack, *J. Geophys. Res.*, *110*, C07021, doi:10.1029/2004JC002293.

Leppäranta, M. (1993), A review of analytical models of sea ice growth, *Atmos. Ocean*, *31*, 123–138.

Light, B., G. A. Maykut, and T. C. Grenfell (2003), Effects of temperature on the microstructure of first-year Arctic sea ice, *J. Geophys. Res.*, *108*(C2), 3051, doi:10.1029/2001JC000887.

Lindsay, R. W. (1998), Temporal variability of the energy balance of thick Arctic pack ice, *J. Clim.*, *11*, 313–331.

Maksym, T., and M. O. Jeffries (2000), A one-dimensional percolation model of flooding and snow ice formation on Antarctic sea ice, *J. Geophys. Res.*, *105*, 26,313–26,331.

Malmgren, F. (1927), On the properties of sea ice, in *The Norwegian North Polar Expedition with the 'Maud' 1918–1925*, vol. 1a no. 5, edited by H. U. Sverdrup, pp. 1–67, John Griegs Boktr., Bergen, Norway.

Martin, S., R. Drucker, and M. Fort (1995), A laboratory study of frost flower growth on the surface of young sea ice, *J. Geophys. Res.*, *100*, 7027–7036.

Maykut, G. A., and N. Untersteiner (1971), Some results from a time-dependent thermodynamic model of sea ice., *J. Geophys. Res.*, *76*, 1550–1575.

Mercier, O. R., M. W. Hunter, and P. T. Callaghan (2005), Brine diffusion in first year sea ice measured by Earth's field PGSE-NMR, *Cold Reg. Sci. Technol.*, *42*, 96–105.

Mundy, C. J., D. G. Barber, and C. Michel (2005), Variability of snow and ice thermal, physical and optical properties pertinent to sea ice algae biomass during spring, *J. Mar. Syst.*, *58*, 107–120.

Nakawo, M., and N. K. Sinha (1981), Growth rate and salinity profile of first-year sea ice in the high Arctic, *J. Glaciol.*, *27*, 315–330.

Nicolaus, M., C. Haas, and J. Bareiss (2003), Observations of superimposed ice formation at melt-onset on fast ice on Kongsfjorden, Svalbard, *Phys. Chem. Earth*, *28*, 1241–1248.

Notz, D. (2005), Thermodynamic and fluid-dynamical processes in sea ice, Ph.D. thesis, 219 pp., Univ. of Cambridge, Cambridge, U.K.

Notz, D., J. S. Wettlaufer, and M. Grae Worster (2005), A non-destructive method for measuring the salinity and solid fraction of growing sea ice in situ, *J. Glaciol.*, *51*, 159–166.

Oertling, A. B., and R. G. Watts (2004), Growth of and brine drainage from NaCl-H$_2$O freezing: A simulation of young sea ice, *J. Geophys. Res.*, *109*, C04013, doi:10.1029/2001JC001109.

Ono, N. (1967), Specific heat and heat of fusion of sea ice, in *Physics of Snow and Ice*, vol. 1, edited by H. Oura, pp. 599–610, Inst. of Low Temp. Sci., Hokkaido, Japan.

Perovich, D. K. (1998), Observations of the polarization of light reflected from sea ice, *J. Geophys. Res.*, *103*, 5563–5575.

Schwarzacher, W. (1959), Pack ice studies in the Arctic Ocean, *J. Geophys. Res.*, *64*, 2357–2367.

Schwerdtfeger, P. (1963), The thermal properties of sea ice, *J. Glaciol.*, *4*, 789–807.

Semiletov, I., A. Makshtas, S.-I. Akasofu, and E. L. Andreas (2004), Atmospheric CO_2 balance: The role of Arctic sea ice, *Geophys. Res. Lett.*, *31*, L05121, doi:10.1029/2003GL017996.

Semtner, A. J. (1976), A model for the thermodynamic growth of sea ice in numerical investigations of climate, *J. Phys. Ocean.*, *6*, 379–389.

Stierle, A. P., and H. Eicken (2002), Sedimentary inclusions in Alaskan coastal sea ice: Small-scale distribution, interannual variability and entrainment requirements, *Arct. Antarct. Alpine Res.*, *34*(4), 103–114.

Sturm, M., J. Holmgren, and D. K. Perovich (2002), Winter snow cover on the sea ice of the Arctic Ocean at the Surface Heat Budget of the Arctic Ocean (SHEBA): Temporal evolution and spatial variability, *J. Geophys. Res.*, *107*(C10), 8047, doi:10.1029/2000JC000400.

Taylor, P. D., and D. L. Feltham (2004), A model of melt pond evolution on sea ice, *J. Geophys. Res.*, *109*, C12007, doi:10.1029/2004JC002361.

Timco, G. W., and R. M.W. Frederking (1990), Compressive strength of sea ice sheets, *Cold Reg. Sci. Technol.*, *17*, 227–240.

Trenberth, K. E., J. G. Olson, and W. G. Large (1989), A global ocean wind stress climatology based on the ECMWF analyses, *NCAR Tech. Note TN-338+STR*, 93 pp., Natl. Cent. for Atmos. Res., Boulder, Colo.

Tucker, W. B., III, A. J. Gow, and J. A. Richter (1984), On small-scale horizontal variations of salinity in first-year sea ice, *J. Geophys. Res.*, *89*, 6505–6514.

Tucker, W. B., III, A. J. Gow, and W. F. Weeks (1987), Physical properties of summer sea ice in the Fram Strait, *J. Geophys. Res.*, *92*, 6787–6803.

Untersteiner, N. (1964), Calculations of temperature regime and heat budget of sea ice in the central Arctic, *J. Geophys. Res.*, *69*, 4755–4766.

Untersteiner, N. (1968), Natural desalination and equilibrium salinity profile of perennial sea ice, *J. Geophys. Res.*, *73*, 1251–1257.

Vancoppenolle, M., T. Fichefet, and C. M. Bitz (2005), On the sensitivity of undeformed Arctic sea ice to its vertical salinity profile, *Geophys. Res. Lett.*, *32*, L16502, doi:10.1029/2005GL023427.

Vancoppenolle, M., T. Fichefet, and C. M. Bitz (2006), Modeling the salinity profile of undeformed Arctic sea ice, *Geophys. Res. Lett.*, *33*, L21501, doi:10.1029/2006GL028342.

Weeks, W. F. (1998), Growth conditions and the structure and properties of sea ice, in *Physics of Ice-Covered Seas*, edited by M. Leppäranta, pp. 25–104, Univ. of Helsinki, Helsinki, Finland.

Weeks, W. F., and S. F. Ackley (1986), The growth, structure and properties of sea ice, in *The Geophysics of Sea ice*, *NATO ASI Ser. B*, vol. 146, edited by N. Untersteiner, pp. 9–164, Springer, New York.

Worster, M. G., and J. S. Wettlaufer (1997), Natural convection, solute trapping and channel formation during solidification of salt water, *J. Phys. Chem. B*, *101*, 6132–6136.

Zillmann, J. W. (1972), A study of some aspects of the radiation and the heat budgets of the Southern Hemisphere oceans, *Meteorol. Stud. 26*, 562 pp., Bur. of Meteorol., Dep of the Inter., Canberra, Australia.

Zubov, N. N. (1945), Arctic ice (in Russian), 217 pp., U. S. Nav. Oceanogr. Off., Bay St. Louis, Miss.

C. M. Bitz, Department of Atmospheric Sciences, MB 351640, University of Washington, Seattle, WA 98195-1640, USA.

M. Vancoppenolle and Thierry Fichefet, Institut d'Astronomie et de Géophysique G. Lemaître, Université Catholique de Louvain, Chemin du Cyclotron, 2, B-1348, Louvain-la-Neuve, Belgium. (vancop@astr.ucl.ac.be)